

CLASSIFICATION OF PLOT-LEVEL FIRE-
CAUSED TREE MORTALITY IN A REDWOOD
FOREST USING DIGITAL
ORTHOPHOTOGRAPHY AND LIDAR

A Thesis Presented to the Faculty of California Polytechnic State
University, San Luis Obispo

In Partial Fulfillment of
the Requirements for the Degree
Master of Science in Forestry Sciences

Brian David Bishop
January 2014

©2014
Brian David Bishop
ALL RIGHTS RESERVED

COMMITTEE MEMBERSHIP

TITLE: CLASSIFICATION OF PLOT-LEVEL FIRE-
CAUSED TREE MORTALITY IN A REDWOOD
FOREST USING DIGITAL
ORTHOPHOTOGRAPHY AND LIDAR

AUTHOR: Brian David Bishop

DATE SUBMITTED: 3/31/2014

COMMITTEE CHAIR: Brian C. Dietterick, Ph.D., P.H.
Director, Swanton Pacific Ranch; Professor of
Hydrology and Watershed Management, Natural
Resources Management and Environmental
Sciences Department

COMMITTEE MEMBER: R. Christopher Olsen, Ph.D.
Professor of Physics and Director, Remote Sensing
Center, Naval Postgraduate School, Monterey, CA

COMMITTEE MEMBER: Steven Rein, Ph.D.
Professor of Statistics, Statistics Department

Abstract

CLASSIFICATION OF PLOT-LEVEL FIRE-CAUSED TREE MORTALITY IN A REDWOOD FOREST USING DIGITAL ORTHOPHOTOGRAPHY AND LIDAR

Swanton Pacific Ranch is an approximately 1,300 ha working ranch and forest in northern Santa Cruz County, California, managed by California Polytechnic State University, San Luis Obispo (Cal Poly). On August 12, 2009, the Lockheed Fire burned 300 ha of forestland, 51% of the forested area on the property, with variable fire intensity and mortality. This study used existing inventory data from 47 permanent 0.08 ha (1/5 ac) plots to compare the accuracy of classifying mortality resulting from the fire using digital multispectral imagery and LiDAR. The percent mortality of trees at least 25.4 cm (10") DBH was aggregated to three classes (0-25, 25-50, and 50-100%). Three separate Classification Analysis and Regression Tree (CART) models were created to classify plot mortality. The first used the best imagery predictor variable of those considered, the Normalized Difference Vegetation Index (NDVI) calculated from 2010 National Agricultural Imagery Program (NAIP) aerial imagery, with shadowed pixel values adjusted, and non-canopy pixels removed. The second used the same NDVI in combination with selected variables from post-fire LiDAR data collected in 2010. The third used the same NDVI in combination with selected variables from differenced LiDAR data calculated using post-fire LiDAR and pre-fire LiDAR collected in 2008. The imagery alone was 74% accurate; the imagery and post-fire LiDAR model was 85% accurate, while the imagery and differenced LiDAR model was 83% accurate. These findings indicate that remote sensing data can accurately estimate post-fire mortality, and that the addition of LiDAR data to imagery may yield only modest improvement.

Acknowledgments

First and foremost, this project could not have happened without the foresight and guidance of The Director, Dr. Brian Dietterick. Russell White provided seemingly endless support and answered more questions than I can ever hope to repay him for, although Spike's hopes I will try. Steve Auten, Shane Larsen, Ben Han, and many others spent many tough hours in the woods, collecting field data for this and other projects. Thanks also to Tom Mastin for his help with surveying and remote sensing, and Dr. Steve Rein for his help with statistics. Both are exceptionally patient in addition to intelligent and knowledgeable, and Cal Poly is lucky to have them. I am grateful to my parents, Jim and Nancy Bishop, for their love and support. Finally, this project is indebted, as am I, to Al Smith, whose generous gift to Cal Poly has changed the lives of so many students.

This project was funded by the USDA McIntire-Stennis and CSU Agricultural Research Initiative grants, and through a grant from the Naval Postgraduate School in Monterey, CA.

Contents

1. Introduction.....	1
1.1 Purpose and need	2
1.2 Objectives	3
2. Background	4
2.1 Study location and site description	4
2.2 Literature Review.....	7
2.2.1 Imagery.....	9
2.2.2 LiDAR.....	14
2.2.3 Fusion of Imagery and LiDAR.....	17
3. Methodology	20
3.1 Field data.....	20
3.2 Imagery	21
3.2.1 QuickBird	22

3.2.2	National Agricultural Imagery Program.....	23
3.2.3	Spry Aerials.....	26
3.3	LiDAR data.....	26
3.4	Plot location adjustment.....	27
3.5	Oversized Plots	28
4.	Analysis and Results	31
4.1	Imagery	33
4.2	LiDAR.....	37
4.4	Salvage harvesting	43
5.	Discussion and Conclusions	46
5.1	Imagery	50
5.1.1	Spry Imagery.....	51
5.1.2	Masking.....	52
5.2	Limitations and sources of error	53
5.2.1	Sample size	53
5.2.3	Spatial accuracy	53
5.2.4	Salvage harvesting	56
5.2.5	Adjustment of NAIP reflectance values.....	56
5.2.6	Errors in mortality data	56
5.3	Recommendations for further study.....	57

Works Cited	59
Appendix A: False-color Infrared Area Map	66
Appendix B: Maps of Estimated Mortality	68
Appendix C: Imagery Georeferencing Accuracy Data	72
Appendix D: LiDAR Height Distributions, scheme B	74

List of Tables

Table 2.1: Study area slopes.....	5
Table 2.2: Common understory species	6
Table 3.1: Average error in positions from imagery	22
Table 3.2: Tasseled Cap Transformation coefficients(Yarbrough et al., 2005).....	23
Table 3.3: R^2 , mortality vs. NDVI, oversized plots	30
Table 4.1: Linear fits, overall and 10" DBH mortality	32
Table 4.2: Plot mortality categories	32
Table 4.3: R^2 and p, linear regression	35
Table 4.4: Confusion matrix, 2010 NAIP unshadowed NDVI	36
Table 4.5: Confusion matrix, 2010 NAIP adjusted NDVI above 2m (scheme A)	36
Table 4.6: Confusion matrix, Imagery and post-fire LiDAR (scheme B)	38
Table 4.7: Confusion matrix, Imagery and differenced LiDAR (scheme C).....	40
Table 4.8: Percent area by mortality class, Lockheed Fire	42
Table 4.9: Percent area by mortality class, clipped to extent of 2008 LiDAR coverage ..	42

List of Figures

Figure 2.1: Study area location	5
Figure 2.2: Harvest history	7
Figure 3.1: Raw pixel values, NAIP 2010 image, unburned sample	24
Figure 3.2: Adjusted pixel values, NAIP 2010 image, unburned sample	25
Figure 3.3: Original & adjusted red and IR bands and NDVI, NAIP 2010 imagery	25
Figure 3.4: Plot 78 tree locations and LiDAR returns	28
Figure 4.1: 2010 NAIP bands 1 and 4 and NDVI, before and after adjustment	34
Figure 4.2: Decision tree for Imagery and post-fire LiDAR (scheme B)	38
Figure 4.3: Decision tree for Imagery and differenced LiDAR (scheme C).....	39
Figure 4.4: Estimated mortality in study area by 3 methods	42
Figure 4.5: Classification metrics vs. mortality by salvage status	44
Figure 4.6: NAIP 2010 adj. NDVI above 2 m vs. QuickBird NDVI.....	45
Figure 5.1: Pixel values from sample of Spry images	52
Figure 5.2: NDVI from sample of Spry images.....	52
Figure 5.3: Illustration of plot errors and areas.....	55

Chapter 1

Introduction

Swanton Pacific Ranch is an approximately 1,300 ha working ranch and forest in northern Santa Cruz County, California, managed by California Polytechnic State University, San Luis Obispo (Cal Poly). The ranch was donated to the school by alumnus Al Smith upon his death in 1994, following a 7-year partnership that involved Cal Poly students and faculty to manage the ranch as a productive, working property and a learning laboratory. Approximately 530 ha of the property is forestland, of which 284 ha are managed for timber production under a Non-industrial Timber Management Plan. The forest is a heterogeneous mixture of a variety of species, dominated by Redwood, Tanoak, Douglas-fir, and Madrone.

In order to support both research and forest management, the forested portion of the ranch has a Continuous Forest Inventory system (CFI), installed partly in 1997 and partly in 2003. The system comprises eighty-three 0.08 ha (1/5 ac) circular plots distributed on a 152.4 m (500 ft) grid.

On August 12, 2009, a fire was ignited to the north of Swanton Pacific Ranch which would come to be known as the Lockheed Fire, and burn 3,163 ha over the course of 11 days. Over one-third of the ranch property was burned, including 300 ha of forestland, representing 51% of the forested area on the property, with variable fire intensity and mortality. Given the existence of high-quality inventory data in the area which had burned, the opportunity existed to evaluate the utility of remote sensing to detect tree mortality resulting from the fire. The two general types of remotely-sensed data which were used in this study are digital multispectral imagery and light detection and ranging (LiDAR).

1.1 Purpose and need

The purpose of this study is to assess how accurately fire-caused tree mortality can be estimated at the stand level from remotely-sensed data in a diverse forested environment. Forest managers have a need for information about fire effects and the spatial distribution of mortality following wildfire, but direct assessment from the field is time-consuming and expensive. Remote sensing may be used to estimate varying levels of mortality and provide a more efficient, timely, scalable, and potentially more cost-effective means for post-fire assessment. Similar past studies have generally used an index of fire 'severity' rather than estimating mortality directly. While useful, estimates of severity are not generally sufficient to make stand-level forest management decisions about post-fire response.

1.2 Objectives

The primary objective of this study is to evaluate the accuracy of a variety of methods for interpreting remote sensing data in estimating percent tree mortality in a forested environment. This is comprised of several smaller objectives:

1. Assess the accuracy of estimates using digital multispectral imagery
 - 1.1. Evaluate a variety of imagery options available to landowners
 1. Compare varying techniques for manipulation of imagery
 - 1.2. Examine the effects of extracting metrics using oversized plots
 - 1.3. Examine the effects of using LiDAR-derived canopy masks
2. Assess the accuracy of estimates fusing post-fire LiDAR data and imagery.
3. Assess the accuracy of estimates fusing pre- and post-fire LiDAR data and imagery.

Chapter 2

Background

2.1 Study location and site description

The study site is a portion of Swanton Pacific Ranch, a 1,320 ha educational and research facility, dedicated to remain a working ranch and forest, owned by the Cal Poly Corporation and managed by the College of Agriculture, Food, and Environmental Sciences at Cal Poly. The ranch is located on the west slope of the Santa Cruz Mountains on the Central Coast of California, approximately 19 km north of the city of Santa Cruz. Elevations across the site range from approximately 20-470 m. The topography is steep and rugged – slopes range from 0-85%, with area by slope class shown in table 2.1. The site experiences a maritime-Mediterranean climate, with cool rainy winters and dry summers, moderated by coastal fog. Average annual rainfall is 77.88 cm.

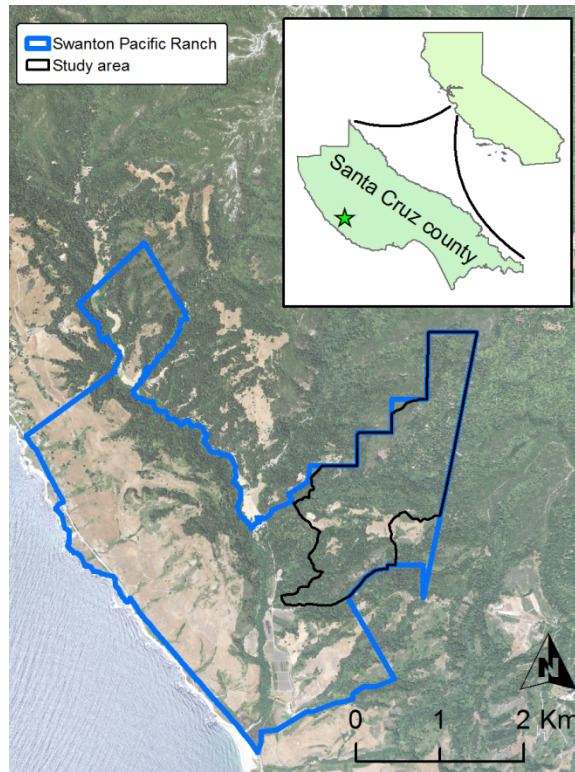


Figure 2.1: Study area location

Table 2.1: Study area slopes

<u>Slope range (%)</u>	<u>Area (%)</u>
< 30	8
30-50	21
50-65	34

Overstory forest canopy in the study area is dominated by second-growth coast redwood (*Sequoia sempervirens* (D. Don) Endl.) with a significant component of Douglas-fir (*Pseudotsuga menziesii* (Mirbel) Franco var *menziesii*), tanoak (*Lithocarpus densiflorus* (Hook & Arn.) Rehder) and coast live-oak (*Quercus agrifolia* (Née)). The riparian is dominated by red alder (*Alnus rubra* (Bong.)) and also has a significant component of bigleaf maple (*Acer macrophyllum* (Pursh)) and California bay

(*Umbellularia californica* (Hook. & Arn.) Nutt.). Understory species are many and varied, but several of the most common are listed in table 2.2.

Table 2.2: Common understory species

<u>Scientific name and authority</u>	<u>Common name</u>
<i>Aralia californica</i> (S. Watson)	Elk-clover
<i>Gaultheria shallon</i> (Pursh)	Salal
<i>Oxalis oregana</i> (Nutt.)	Redwood sorrel
<i>Polystichum munitum</i> (Kaulf.) C. Presl.	Western sword fern
<i>Rubus parviflorus</i> (Nutt.)	Thimbleberry
<i>Rubus ursinus</i> Chan. & Schtdl.	California blackberry
<i>Toxicodendron diversilobum</i> (Torr. & A. Gray) Greene	Poison-oak
<i>Trillium ovatum</i> (Pursh)	Western trillium
<i>Urtica dioica</i> L. subsp. <i>Gracilis</i> (Aiton) Selander	Stinging nettle
<i>Vaccinium ovatum</i> (Pursh)	Huckleberry

With the exception of a small stand at the northernmost extent, the entire study site was clearcut in the early 20th century. Portions of the site were salvage logged following the Pine Mountain Fire in 1948. Approximately 127 ha, 41% of the site, was selectively harvested between 1989-2008, with some portions harvested twice within this period. As a result, the structure of the forest is variable across the site, with 1-3 age classes present. Basal area (BA) within the plots range from 4-202 m²/ha; BA within plots used for this project range from 35-124 m²/ha. The entire site is located within the perimeter of the Lockheed fire. As a result of the fire, 37.5 hectares of the study area were salvage-logged using a helicopter in the winter of 2009 (see figure 2.2).

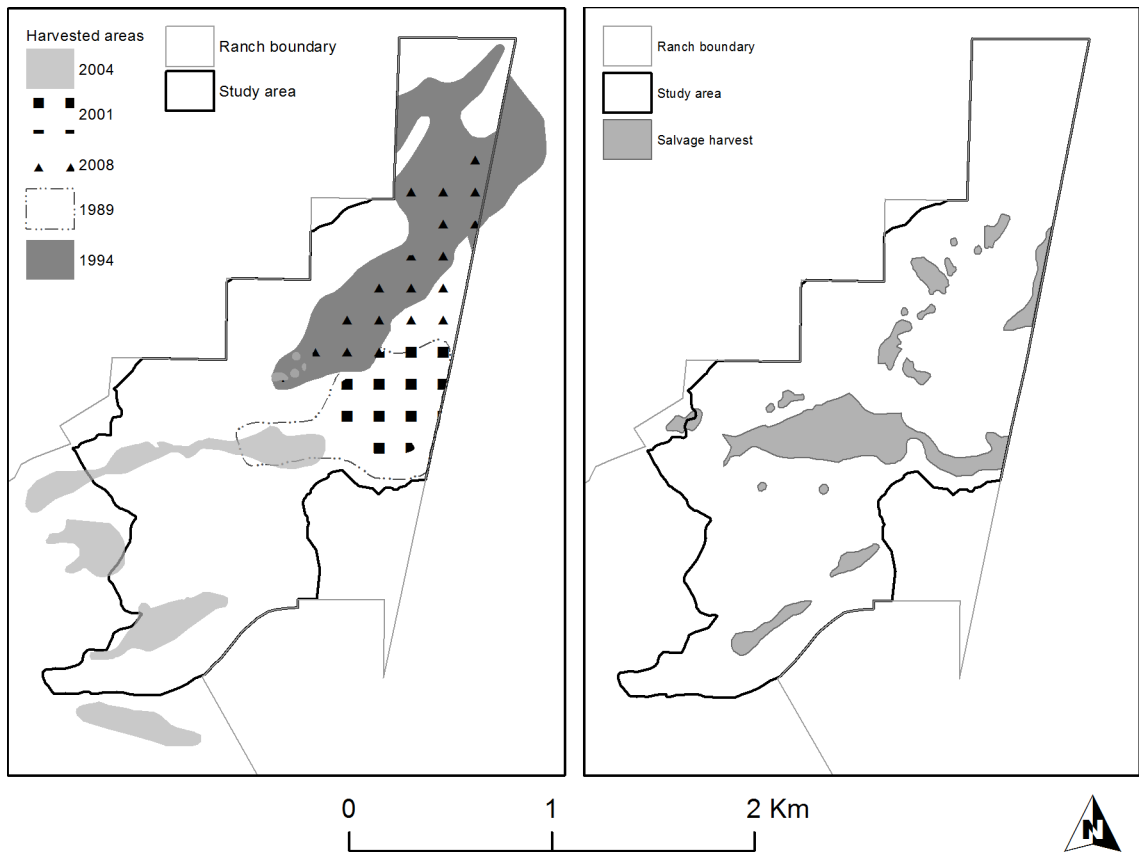


Figure 2.2: Harvest history

2.2 Literature Review

Wildland fires burn with varying intensity, which may be measured as flame height, heat, rate of spread, or total energy released. The resulting effects depend on the interaction of intensity and duration with ecological characteristics of the site, and are commonly referred to as fire severity. Although there is no common standard for ecological measurement of fire severity, one field measurement which is applicable across a wide range of vegetation types and has gained relatively widespread acceptance is composite burn index (CBI). CBI rating comprises the condition and color of soil,

amount of vegetation consumed, scorch of trees, and presence of sprouting and/or new colonizing vegetation (Key & Benson, 2006). Other measures may be used where they are perceived to be more relevant to the goals of land managers – for example, amount of vegetation removed (Fox, Maselli, & Carrega, 2008), change in leaf area index (Δ LAI) (Boer et al., 2008), change in vegetation height (Kaufmann, Stoker, & Greenlee, n.d.), or mortality (Kobziar, Moghaddas, & Stephens, 2006; Rogan & Yool, 2001).

The changes to the structure and color of aboveground vegetation and the color of soil result in changes in the signal returned by both active and passive remote sensing systems. In particular, discrete-return light detection and ranging (LiDAR) and digital orthophotography are commonly used to assess of the condition of vegetation, including change detection following disturbance events, such as wildland fire. The use of imagery to detect and characterize tree mortality and severity of forest fires has a more robust history. CBI was developed for use in mapping burn severity using Landsat TM/ETM 30m imagery (Key & Benson, 2006). Accuracy, however, can be an issue, as “countervailing post-fire factors often lead to spectral confusion” (Rogan & Yool, 2001). LiDAR is a relatively new technology, and few studies have attempted to use LiDAR to detect or characterize damage resulting from forest fire, although pre- and post-fire LiDAR datasets have been used to detect areas where vegetation was entirely removed by fires (Kaufmann et al., n.d.; Wang & Glenn, 2009). The increasing use of LiDAR to describe aboveground biomass, however, is well documented in scientific literature (Carson, 2004; Lefsky, Cohen, Parker, & Harding, 2002; Lim, Treitz, Wulder, St-Onge, & Flood, 2003; Renslow, 2000). LiDAR data have been used to estimate plot- or stand-level metrics such as Lorey's mean height, volume (Goerndt, Monleon, & Temesgen, 2010)

and quadratic mean diameter (Goerndt et al., 2010; Muss, Mladenoff, & Townsend, 2011), as well as to characterize stand characteristics such as successional stage (Falkowski, Evans, Martinuzzi, Gessler, & Hudak, 2009), presence of understory (Hill & Broughton, 2009; Maltamo et al., 2005; Martinuzzi et al., 2009), and snags (Martinuzzi et al., 2009). This review is divided into three sections: Imagery, LiDAR, and Fusion (the use of imagery and LiDAR techniques together to produce a single classification or model).

2.2.1 Imagery

There are a variety of strategies for characterizing the effects of disturbance events using one or more digital orthophotos, and many have been applied to characterize vegetation changes after wildland fire. Most broadly, these break down into change detection using before and after (multi-temporal) scenes versus single-scene methods. Commonly used methods (in both categories) are linear transformations, univariate image differencing, and supervised, unsupervised, and hybrid classification (Coppin, Jonckheere, Nackaerts, Muys, & Lambin, 2004; Lu, Mausel, Brondízio, & Moran, 2004).

The most commonly used strategies are methods of univariate image differencing (Coppin et al., 2004). Within this umbrella, one strategy which has been used to assess burn severity is the comparison of band ratios before and after wildland fire. Two commonly used indices based on band ratios are the normalized burn ratio (NBR) and the normalized difference vegetation index (NDVI), their multi-temporal counterparts are differenced normalized burn ratio (dNBR) and differenced normalized difference vegetation index (dNDVI). dNBR was originally defined based on Landsat TM/ETM bands 4 and 7 – near-infrared (NIR) and short-wavelength infrared (SWIR). NIR values

tend to decrease, and SWIR to increase, pre-fire to post-fire, and the change in these bands is greatest in magnitude of all bands. Of all bands, SWR exhibits the greatest variance when considering values for burned areas. Scaling by the sum of bands normalizes for overall brightness, and helps remove topographic effects. Thus, normalized burn ratio is defined as $(NIR - SWIR)/(NIR + SWIR)$, and dNBR as $NBR_{\text{prefire}} - NBR_{\text{postfire}}$. dNBR is positive over areas of productive vegetation; near zero for clouds, cured grasses, soil, and rock; and negative for severe water stress and nonvegetative traits created within burn areas (Key & Benson, 2006). Similarly, NDVI is defined as $(NIR - RED)/(NIR + RED)$, and dNDVI as $NDVI_{\text{prefire}} - NDVI_{\text{postfire}}$.

Although dNBR may be more sensitive to changes caused by wildland fire, NDVI can be calculated from a wider variety of imagery, which may be available at finer spatial and temporal scales than Landsat imagery. A comparison of six approaches (two artificial neural networks, two principal component analyses, NDVI, and two differenced band ratios, one of which is dNBR) demonstrated that dNBR produces similar results to much more complicated methods (C. Kenneth Brewer, J. Chris Winne, Roland L. Redmond, David W. Opitz, & Mark V. Mangrich, 2005). The dNBR method, applied to Landsat imagery, is used operationally by the US Forest Service Remote Sensing Applications Center to support burned area emergency response following major wildland fires across the US. There is 73-75% agreement between dNBR and composite burn index (CBI). In correlating dNBR and CBI, most (32%) of the errors were confusion between unburned and low-severity areas, and high severity areas had the lowest rate of error in two years of assessment (Cocke, Fulé, & Crouse, 2005). However, in a Redwood and Tanoak forest following the Big Sur Basin Complex Fire, linear models based on Landsat TM bands

(3,4,5,7) and (2,3,4) respectively were better predictors of overall CBI and damage to dominant trees, than dNBR (Meng & Meentemeyer, 2011). A comparison of eight indices (four single scene, and their multi-temporal companions) for the detection of burn severity in a ponderosa pine forest in South Dakota found that dNDVI outperformed dNBR at year one assessment, while dNBR performed better at extended assessment (years 2, 3, 5, and 7) when compared to CBI (Chen et al., 2011). Comparison of NDVI and dNBR from Landsat TM/ETM+ scenes across four wildfire burn sites in Alaska to CBI found that NDVI performed similarly to dNBR (lrl of .72 vs. .70) (Epting, Verbyla, & Sorbel, 2005). Assessment of fire severity across three fires in pine, oak, and eucalyptus forests in Spain found that NDVI performed similarly to NBR, dNDVI similarly to dNBR, and that single-scene indices outperformed multi-temporal indices at describing severity within burned areas, while multi-temporal indices were more accurate at distinguishing between burned and unburned areas (Escuin, Navarro, & Fernández, 2008). Using SPOT imagery to map burn severity with an eye toward increased runoff resulting from reduced vegetative cover following wildland fire in an oak/pine forest in France, NBR and NDVI values were found to be strongly correlated, as were dNBR and dNDVI. In this case, multi-temporal images performed better than single scenes, due to inclusion of areas of bare rock and vineyards in the study area (Fox et al., 2008). Burned pine/broadleaf forestland in Korea was classified to four classes (including unburned) with 83% overall accuracy (kappa = .76) using dNDVI from Landsat TM imagery (Lee, Kim, Chung, & Park, 2008).

Change in leaf area index (Δ LAI) is another potential measure of burn severity, which can be measured in the field and via remote sensing. Following wildland fire in a

Jarrah (*Eucalyptus marginata*) forest in SW Australia, Δ LAI was similarly related to NBR, NDVI, and the simple ratio (SR), $\frac{NIR}{RED}$, from Landsat TM imagery ($R^2 = 0.87$ for all). Of the three methods, SR was the most accurate at detecting burned areas, while NBR and NDVI both had errors of commission outside the burn perimeter (Boer et al., 2008).

Another set of strategies commonly used with imagery are transformations, generally the principal components (PC) transformation and the Kauth-Thomas or tasseled cap transformation. PC transformation is a statistical method, which uses orthogonal transformation to derive a set of linearly uncorrelated variables, where the first variable describes the greatest possible variance among the bands (generally, this is essentially overall brightness), and each successive variable describes the greatest variance possible, subject to the constraint of orthogonality. The resulting bands do not correspond to any particular features in the scene. The Kauth-Thomas (KT) or tasseled cap transformation was originally developed for agricultural applications using Landsat MSS data (Kauth & Thomas, 1976). Similarly to PC transformation, it is an orthogonal transformation, however, the coefficients used to project original bands onto ‘tasseled-cap space’ are designed to bring out specific physical features within imagery – namely, ‘brightness’, ‘greenness’, ‘wetness’, and ‘other’ (the last coordinate is chosen to be orthogonal to the first three but does not represent any particular feature). Tasseled-cap coefficients have been developed for other sensors, including the QuickBird satellite (Yarbrough, Easson, & Kuszmaul, 2005). Kauth-Thomas linear transformation techniques and principal component analysis both enhance the utility of Landsat TM imagery for detection and classification of burned forest areas. In general, KT provides

superior accuracy of classification of burn severity (17% better accuracy compared to PC). In particular, KT is more sensitive to greenness and wetness (i.e. differences in vegetation and moisture). Accuracy of both KT and PC analysis was greatest for most severe, then moderate, and least for least severely burned areas (Patterson & Yool, 1998; Rogan & Yool, 2001).

Unsupervised classification relies on statistical methods to delineate areas whose signatures (collected band values, without band differencing or ratioing) are the most dissimilar. Using unsupervised classification, only the number of classes is specified; the classes and pixels that belong to them are identified by software. Alternatively, supervised classification is conducted by a user with a priori knowledge of conditions on the ground. Known regions representing each class are provided as input to the classification software, which evaluates the entire area of interest and assigns each pixel to the class with which it is most closely associated. Automated maximum-likelihood classification of six-band imagery was used to delineate areas of red discoloration caused by jack pine budworm in a Canadian forest, with average commission accuracy of 86%. Adding separately obtained infrared imagery did not improve the accuracy (Leckie, Cloney, & Joyce, 2005). There are also methods which hybridize both approaches: A hybrid of unsupervised classification, spectral unmixing, and object-based classification techniques was used with a high resolution digital multispectral image to detect presence/absence of solitary standing dead trees in a hardwood-dominated forest in Canada. Accuracy was 94% (47/50) for areas classified as dead wood, and 70% for areas classified as having no dead wood present (Pasher & King, 2009). A hybrid of supervised and unsupervised classification was 93.2-95% accurate in recognizing trees killed by

sudden oak death on two forested sites (one oak woodland, one redwood and tanoak) in Marin County, CA from 1m 4-band imagery. The hybrid method outperformed both pure supervised and pure unsupervised classification, which had similar performance (Kelly, Shaari, Guo, & Liu, 2004).

Regardless of which modeling/classification strategy is used, if multiple scenes will be used, the dates on which pre- and post-fire imagery are acquired is important. Unburned features in the landscape are altered by wetting and drying, and productivity cycles. Pre- and post-fire acquisitions should have as similar moisture content and phenology as possible. In general, early to middle growing season periods have the best results. NDVI tends to degrade late in the growing season more than dNBR. In order to match phenology, pre-fire imagery should generally come from a prior year, unless it can be obtained within 24 days of the post-fire image (without significant change in conditions). Extended assessment (post-fire scene obtained from the following growing season instead of immediately following fire) may be more representative of actual severity (Key & Benson, 2006).

2.2.2 LiDAR

A variety of strategies have been used to model stand-level metrics based on attributes of LiDAR data. In a Douglas-fir/Grand Fir forest in Oregon, LiDAR data with average first-return density of 10 points/m² was used to estimate BA, Lorey's mean height, volume, density, quadratic mean DBH, and crown width using both area-based and single-tree approaches. The area-based approach was best for BA ($R^2 = 89.7$), volume (90.4), density (91.9), quadratic mean DBH (82.1), crown width (79.9). The single-tree approach was best for Lorey's mean height ($R^2 = 96.4$). Area models

performed as well or better than single-tree models except for Lorey's mean height. LiDAR metrics used in best models included max, mean, percentiles, and interquartile distances in canopy heights; a variety of normalized point densities in height bins; and median, maximum, and percentiles of intensity data (Goerndt et al., 2010). Aggregations of LiDAR hits over 2-60m radius plots can be used to generate cubic-spline pseudo-waveforms of height/intensity and height/frequency data. There does not appear to be any justification for the pseudo-waveform technique with intensity data, but wave-based models based on frequency may be more plausible. Comparing frequency-based and frequency-waveform models, of 11 parameters modeled, 5 (highest canopy point in plot, crown base height, log of mean stem diameter, log of aboveground biomass, and log of foliage biomass) were best modeled by frequency; 5 (average canopy height, crown length, canopy coverage, log of total stand basal area, and log of total stand stem density) were best modeled by frequency-based waveform, and one (log of branch biomass) was equally well modeled by both. The average increase in R^2 for parameters modeled better by waveform method was .064, while the average increase in R^2 for parameters modeled better by frequency was .038 (Muss et al., 2011).

Thematic classification of stands has also been attempted using LiDAR data. A random forest algorithm was used with LiDAR data (density of 0.26 returns/m²) to classify a multi-species conifer forest in Idaho by forest successional stage. In one model, with 7 classes, having overall accuracy of 90.12%, canopy cover and mean height were the most important predictors, followed by the density in two height strata from 1-2.5m and 20-30m, median height, 25th percentile height, modal height, and density in the 10-20m height stratum. In another model, with 6 classes, having overall accuracy of

95.54%, canopy cover and mean height were the most important predictors, followed by maximum height, median height, and density of the 20-30m height stratum(Falkowski et al., 2009).

In a fashion somewhat similar to classification strategies, LiDAR data have been used to detect the presence or absence of particular conditions in forested environments. The presence of understory vegetation in a diverse deciduous forest, for example, was detected by filtering leaf-on and leaf-off LiDAR data based on probable height to crown base by species of overstory tree cover, with 77% accuracy using both datasets, and 72% accuracy using only leaf-off data (Hill & Broughton, 2009). This was accomplished using relatively low-density data - 1 pulse/m². An algorithm based on kernel-filtered height histogram of laser hits was able to correctly detect the presence/absence of multistory forest condition in 24 of 28 plots in a mixed conifer forest in Finland. A model based on proportion of vegetation hits (essentially, ground return ratio), 20th percentile canopy height, maximum LiDAR height, and natural log of 60th percentile canopy height was able to predict the logarithmic number of understory trees with R² of .87 (Maltamo et al., 2005). The distribution (presence/absence) of shrub understory was mapped with 83% accuracy in a mixed conifer forest in Idaho using percent ground returns, percent of returns between 1 and 2.5m, and plot slope multiplied by the cosine of aspect, and the distribution (presence/absence) of snags was mapped with 72-80% accuracy using a variety of topographic and canopy height metrics derived from LiDAR (Martinuzzi et al., 2009). In a forest with a relatively high component of standing dead trees, on the north rim of the Grand Canyon, LiDAR percentile heights and high/low intensity peak frequency data was used to distinguish between live and standing dead biomass and

estimate volume of each with R^2 of 0.76 for live biomass, and 0.62 for dead (Kim et al., 2009).

While LiDAR has been used more extensively to characterize forest stand conditions in general, relatively few studies have used LiDAR data to describe or quantify damage resulting from forest fires. Canopy height (first return – bare earth) changes from LiDAR data gathered before and after the Hayman Fire in Colorado revealed areas where vegetation was consumed, but errors in repeated measurement confounded quantification of vegetation lost (Kaufmann et al., n.d.). In sagebrush vegetation, damage was estimated from change in height of first return. Accuracy of classification by this method ranged from 64-96%, and was superior to classification by dNBR, which ranged from 32-85% (Wang & Glenn, 2009).

2.2.3 Fusion of Imagery and LiDAR

Fusion of imagery and LiDAR techniques discussed above has been used for a similar variety of purposes. These strategies may be as simple as utilizing information from both datasets (sometimes referred to as 'stacking'), but often involves linear transformations of combined data, machine-learning algorithms, supervised classification, or some hybrid combination of any of the preceding methods. The use of NDVI from a 0.5 m color infrared ortho-image to identify shrub cover on an experimental site in Portugal improved the accuracy of a DEM created from simultaneously captured LiDAR data, which improved the estimation of shrub canopy height ($R^2 = 0.65$ vs. 0.48). A variety of fuel metrics (canopy height, basal area, canopy cover, shrub cover, shrub height) were modeled in a Sierra Nevada mixed conifer forest with R^2 between .87-.59 using principal component analysis of NAIP 1 meter 4-band

imagery and heights, percentiles, and densities from LiDAR data having average pulse density of 9 pulses/m² (Jakubowski, Guo, Collins, Stephens, & Kelly, 2013). Support vector machines, a machine-learning algorithm, outperformed simple regression for modeling fuel loads, while simple regression was adequate for simple tree metrics, when using principal component analysis of NAIP 1 meter 4-band imagery and heights, percentiles, and densities from LiDAR data having average pulse density of 9 pulses/m² in a Sierra Nevada mixed conifer forest (Jakubowski et al., 2013). Minimum noise fraction, a variation of principle component transformation, outperformed simpler principle component analysis (90.1% accuracy, k=0.86 vs. 61.4% accuracy, k=0.52) and “stacking” (using LiDAR-derived canopy cover, canopy height model variance, and normalized point density in four 0.5m height bins as bands in a raster with the imagery, without transformation)(87.2% accuracy, k=0.863) at modeling surface fuels (9 models/classes) in pine-hardwood forestland including areas of brush and grass in east Texas (Mutlu, Popescu, Stripling, & Spencer, 2008). Supervised classification based on a minimum noise fraction transformation of QuickBird 2.5m 4-band imagery and LiDAR-derived canopy cover, canopy height model variance, and normalized point density in 10 height bins of 0.5-5m was able to model surface fuels in pine-hardwood forestland including areas of brush and grass in east Texas (using 9 classes) with 90.1% accuracy (k=0.86) (Mutlu et al., 2008).

Fusion of LiDAR and imagery has also been used to classify forestland as to stand structure or other characteristics. Principal component analysis of 2' resolution color infrared imagery and a variety of metrics derived from LiDAR data with 2.5-27 points/m² were used to classify a redwood forest into 36 strata (Golinkoff, Hanus, & Carah, 2011).

Principal component analysis of NAIP 1 meter 4-band imagery and heights, percentiles, and densities from LiDAR data having average pulse density of 9 pulses/m² was able to classify a Sierra Nevada mixed conifer forest with regards to 40 surface fuel models with 45% accuracy, and a broader classification of 3 surface fuel types with 73-76% accuracy (Jakubowski et al., 2013).

Chapter 3

Methodology

3.1 Field data

There are 83 CFI plots distributed across the study area. Fifty of these 0.08 ha (1/5 ac) circular plots were installed in 1997 and re-measured in 2008, and the remaining 33 installed in 2003. The plots were installed on a 152.4 m (500 ft) grid established by Maskrey and Reimer in 1993, which is tied to USGS benchmark 1238N, located on the Little Creek Bridge on Swanton Road, that point having the assumed local coordinates (10,000' N; 10,000' E) for the purposes of the inventory system. Plot locations were established based on a variety of control points set along the Little Creek haul road, using a staff compass and cloth tape. As a result, the plots are not located precisely along the theoretical true North-South grid or at precisely 500 ft spacing, with the errors in locations increasing with increasing distance from survey control. During subsequent plot

re-measurements, positions were collected at plot centers using a Garmin 60csx GPS in 2009 (except for one plot, a GPS position for which was collected in 2013).

A variety of standard forest inventory data is collected every ten years at each CFI plot, however, data used in this analysis was limited to tree species, DBH, bearing and distance from plot center, and tree status (live or dead). Tree status was assessed each year following the fire, through 2012, with the most recent (2012) status being used for this analysis, while DBH was measured in either 2003 or 2008 (for plots established in 1998). The diameters of trees in plots measured in 2003 was projected to 2008 using a growth rate of 2% (Auten, 2012). For further description of field methods, see Bonner (1998), Anderson (2003), Maskrey and Reimer (1993), and Auten (2012).

3.2 Imagery

Three sets of digital multispectral imagery were available for this project: Digital Globe's QuickBird satellite imagery, aerial photos taken as part of the National Agricultural Imagery Program (NAIP), and aerial photos taken by Kevin Spry (Spry Aerials). The accuracy of georeferencing of imagery used was checked by determining the coordinates of two buildings which could be seen and whose locations had been surveyed using a total station. The average error across the two locations checked is shown in table 3.1, and the supporting information in appendix B.

Table 3.1: Average error in positions from imagery

<u>Image</u>	<u>Average Error (ft)</u>
NAIP 2009	3.265
NAIP 2010	8.32
NAIP 2012	8.38
QuickBird 2008	31.435
QuickBird 2009	99.42
Spry 2010	3.81

3.2.1 QuickBird

QuickBird images from 10/13/2008 (pre-fire) and 9/15/2009 (post-fire) were obtained for this project. The spatial resolution of these images is 2.4m for color and infrared, with a 60cm panchromatic band. NDVI was calculated for both images, and $dNDVI$ calculated as $NDVI_{postfire} - NDVI_{prefire}$. In order to examine whether masking out areas of the imagery which did not contain forest canopy would improve the relationship with mortality, a series of canopy masks was made by subtracting the LiDAR DEM from the canopy surface model, and reclassifying the resulting canopy height mask (CHM) raster to a binary mask based on canopy height. Masks were made for 1-5 m heights, and used to create canopy-masked NDVIs at each height, where areas of the raster with CHM values below the threshold height had their pixel values replaced with 'NoData'. The post-fire image was also transformed into tasseled cap space using the coefficients shown in Table 3.1, derived by Yarbrough, Easson, and Kuzmaul.

Table 3.2: Tasseled Cap Transformation coefficients(Yarbrough et al., 2005)

	<u>Brightness</u>	<u>Greenness</u>	<u>Wetness</u>	<u>Other</u>
Blue	0.319	-0.121	0.652	0.677
Green	0.542	-0.331	0.375	-0.675
Red	0.49	-0.517	-0.639	0.292
Infrared	0.604	0.78	-0.163	0.011

All of the aforementioned processing was performed, and average plot values for NDVI, the four canopy-masked NDVIs, dNDVI, and the four Tasseled Cap bands were extracted, in ArcMap 10.1.

3.2.2 National Agricultural Imagery Program

Orthoimages covering the project area were obtained by downloading digital ortho-quarter-quads taken in the summers of 2009, 2010, and 2012, and stitching them together in ArcMap 10.1. The spatial resolution of these images is 1m. NDVI was calculated for all three images, and dNDVI calculated as $NDVI_{2010} - NDVI_{2009}$ and as $NDVI_{2012} - NDVI_{2009}$. The 2010 image has extensive deep shadows, which, in preliminary exploration of the data, interfered with the relationship between NDVI and mortality. Two different techniques were explored in an attempt to get the most out of the data: using only unshadowed pixels, and adjusting the values of shadowed pixels. The first step for both techniques was an unsupervised classification process in ArcGIS, with 7 classes, 2 of which corresponded with shadowed pixels. The resulting raster was reclassified to a set of masks, one having value 1 for unshadowed areas, and NoData for shadowed areas, and the other having value 1 for shadowed areas, and NoData for unshadowed areas. These masks were used to extract average plot values of NDVI and dNDVI, from only shadowed or unshadowed pixels. They were also used to extract

samples of unshadowed and shadowed pixels from an unburned portion of the scene, with similar vegetation as the fire area. Approximately 20 million unshadowed pixels and approximately 8 million shadowed pixels were compared. The distributions of pixel values from the sample are shown below in figure 3.1.

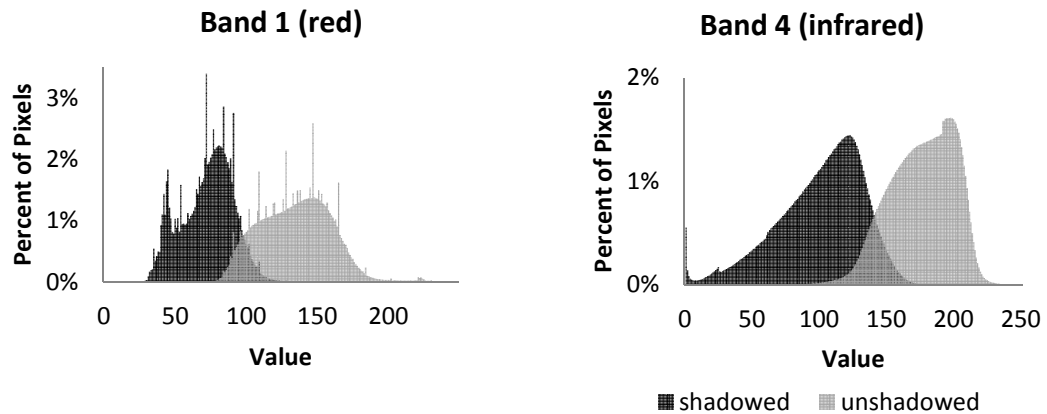


Figure 3.1: Raw pixel values, NAIP 2010 image, unburned sample

The mean values of each sample of pixels were calculated. For band 1, the mean value of shadowed pixels was 73, while the mean value for unshadowed pixels was 135. For band 4, the mean value of shadowed pixels was 101, while the mean value for unshadowed pixels was 177. The values of shadowed pixels were adjusted by the difference in means (62 for band 1, and 76 for band 4). The resulting distributions, shown in figure 3.2, are very similar.

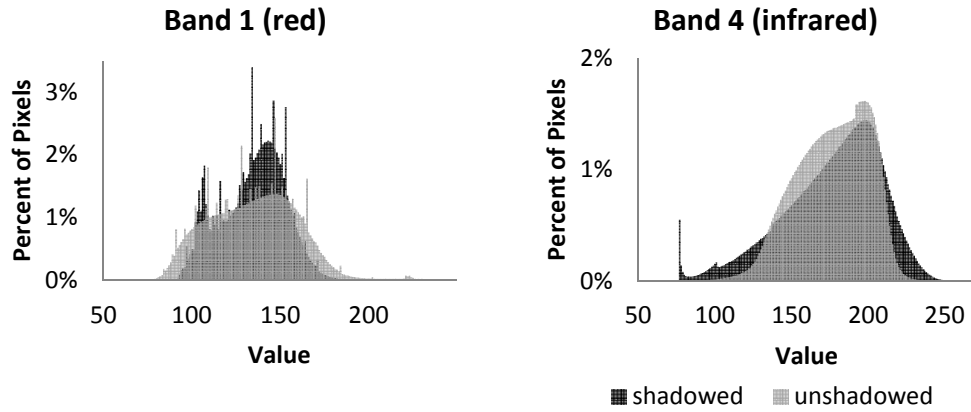


Figure 3.2: Adjusted pixel values, NAIP 2010 image, unburned sample

The resulting NDVI, along with individual bands, are shown in figure 3.3, along with the originals. The variability in the adjusted NDVI across the study area is much greater than in the original, although the overall range is very similar.

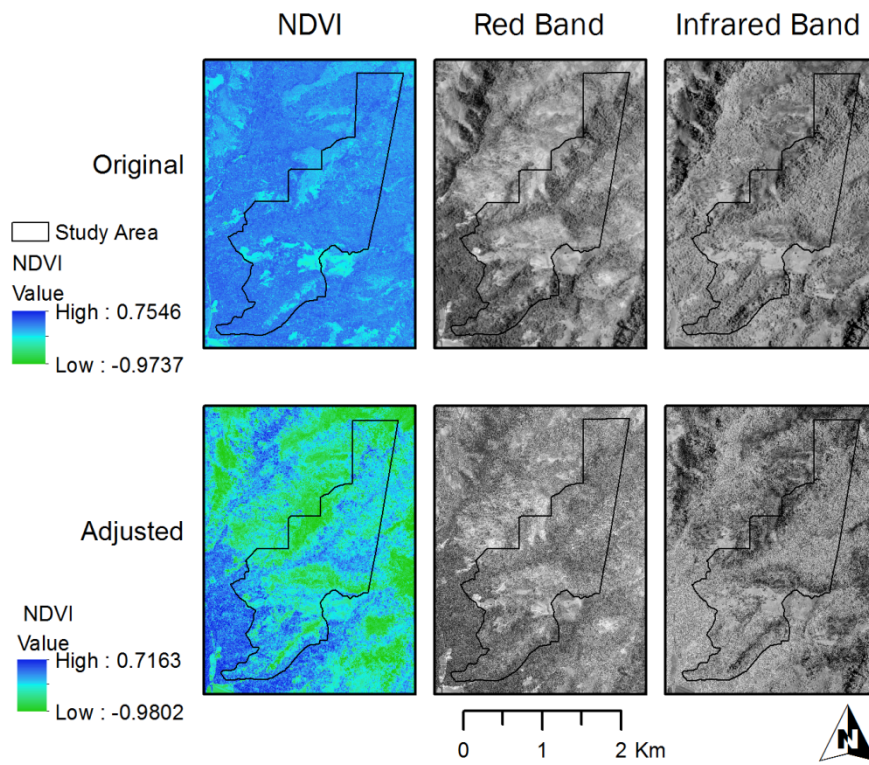


Figure 3.3: Original & adjusted red and IR bands and NDVI, NAIP 2010 imagery

In the same fashion as the QuickBird imagery, canopy-masked NDVI rasters were created at 1-5 m threshold heights for unshadowed and adjusted NDVI. Average plot values for 2010 NDVI, dNDVI, unshadowed NDVI, adjusted NDVI, and for twelve total canopy-masked unshadowed and adjusted NDVIs were calculated in ArcMap 10.1. Average plot values for 2012 NDVI and dNDVI were also calculated in ArcMap 10.1.

3.2.3 Spry Aerials

These images were taken at an average altitude of 4,234 m AMSL, using a Vexcel UltraCam X, by Kevin Spry (www.geog2.com). The spatial resolution of these images is 29.2 cm. Post-fire imagery was captured during the summer each year following the fire, on 6/13/2010, 7/27/2011, and 5/11/2012. Normalized Difference Vegetation Index was calculated for all three images in ArcGIS.

3.3 LiDAR data

Two LiDAR data sets were used for this project: one collected February 28-29 2008, and one March 9-10 2010, both by Airborne1 corporation, El Segundo CA. The 2008 flight used an Optech ALTM 3100 sensor aboard a Cessna 210 fixed-wing aircraft, scanning at 100,000 Hz with a scan angle of 14°. The 2010 flight used an Optech ALTM Orion sensor aboard a Navajo Chieftain fixed-wing aircraft, scanning at 150,000 Hz with a scan angle of 14°. For both flights, 1-sigma horizontal accuracy was 30 cm, and vertical accuracy 18.3 cm at 95% confidence and 15.2 cm at 90% confidence, according to the vendor. Quality assurance for elevations was provided by the vendor using real-time kinematic GPS points. For the 2008 flight, 1,046 points were collected; RMSE for the

LiDAR DEM was 0.03 m, with residuals ranging from -0.15 to 0.07 m. For the 2010 flight, 2,742 points were collected; RMSE for the DEM was .034 m, with residuals ranging from -0.052 to 0.03 m. Raw data from both flights were delivered in LAS format, filtered by the vendor to identify bare-earth ground returns, and with points classified as first, last, or intermediate returns. Average first-return density across the study area was 5.78 returns/m² for the 2008 data and 8.12 returns/m² for the 2010 data. The raw LiDAR data were clipped to the locations of the CFI plots and exported as comma-separated value files using FUSION LiDAR toolkit, developed by the US Forest Service. Height percentiles and a variety of other metrics describing the vertical distribution of LiDAR returns above 2 m, as suggested by White et. al. (2013) in their best-practices guide, were calculated for each plot using the CloudMetrics tool in FUSION. The number of points in 1 m height bins was calculated for each plot using the DensityMetrics tools in FUSION. Height percentiles were normalized by mean and mode, and point counts in 1 m height bins were normalized by total number of points, in Microsoft Excel.

3.4 Plot location adjustment

In an attempt to increase the accuracy of mapped plot locations, a stem map was created from bearings and distances collected for each CFI plot, and estimated heights based on allometric equations for redwood and douglas-fir (Eng, 2012). The stem map was visualized along with the portions of the LiDAR point cloud in and around the plots in ArcScene, as shown in figure 3.4. Of 47 plots whose location was examined, 17 appeared to be correctable, while 15 appeared to be correct, and the remaining 15 could not reasonably be corrected in this fashion. Of the plots which had their locations adjusted, the average adjustment was approximately 12.5m. Including plots whose

locations were considered correct, the average adjustment was approximately 8.6m. Average values were extracted from the NAIP 2010 unshadowed NDVI image and the 2009 QuickBird NDVI using both the unadjusted and adjusted plot locations. There was no improvement in the relationships between NDVI and mortality based on the adjustment, so, in the interest of consistency, the original unadjusted locations were used for all further analysis.

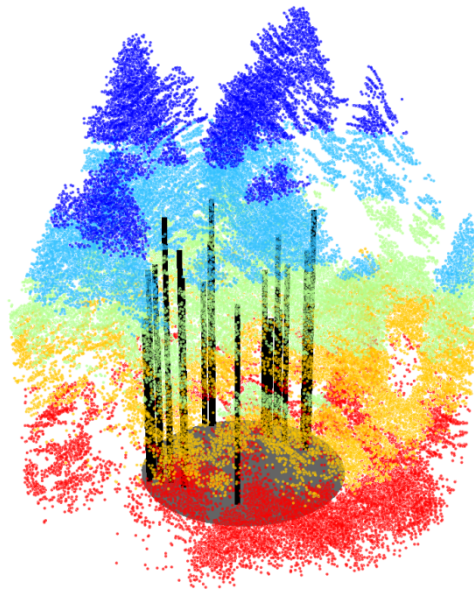


Figure 3.4: Plot 78 tree locations and LiDAR returns

3.5 Oversized Plots

In order to determine the optimal size for extracting information from imagery (and possibly LiDAR), NDVI from the 2010 NAIP unshadowed, including two canopy-height-masked, NDVIs; 2010 NAIP adjusted, including two canopy-height-masked; and QuickBird imagery was extracted for 1, 2, and 3 m buffers on the plot areas (yielding plot areas of 0.09, 0.10, and 0.11 ha compared to the original 0.08 ha). In implementing a

forest inventory using variable-plot sampling with a 20 BAF prism, resulting in a median 'plot size' of 0.036 hectares (, Golinkoff et al. determined that a .08 ha grid cell was the optimal size for extraction (Golinkoff et al., 2011). Intuitively, it seems plausible that extracting information from a slightly oversized plot should, at a minimum, not decrease accuracy, since trees near the edges of plots will have a significant portion of their crowns outside the plot, and since the intensity of a fire in the area immediately adjacent to a plot will have an effect on the mortality within that plot. Average NDVI from the eight combinations of imagery and plot size were used as predictors in linear regression. The results, shown in table 3.2, do not strongly support the use of oversized plots for extraction. All three unshadowed NDVIs demonstrate a slight decrease in the strength of the relationship with mortality, as does the QuickBird NDVI. All three adjusted NDVIs show modest improvement in the relationship at one and two meters, and then a small decrease at three meters. Given the additional workload associated with extracting LiDAR variables for a series of buffered plots, and the complexity of translating the concept into wall-to-wall prediction, oversized plots were not used for this project.

Table 3.3: R^2 , mortality vs. NDVI, oversized plots

<u>Model</u>	<u>R-squared</u>
NAIP 2010 unshadowed NDVI	0.48
1m buffer	0.476
2m buffer	0.474
3m buffer	0.47
NAIP 2010 unshadowed NDVI above 1m	0.496
1m buffer	0.495
2m buffer	0.495
3m buffer	0.494
NAIP 2010 unshadowed NDVI above 2m	0.496
1m buffer	0.495
2m buffer	0.494
3m buffer	0.493
NAIP 2010 shadow-adjusted NDVI	0.487
1m buffer	0.49
2m buffer	0.492
3m buffer	0.49
NAIP 2010 shadow-adjusted NDVI above 2m	0.516
1m buffer	0.52
2m buffer	0.522
3m buffer	0.521
NAIP 2010 shadow-adjusted NDVI above 5m	0.524
1m buffer	0.528
2m buffer	0.53
3m buffer	0.529
QuickBird NDVI	0.373
1m buffer	0.359
2m buffer	0.359
3m buffer	0.346

Chapter 4

Analysis and Results

Initial, exploratory analysis was performed using linear regression and imagery, which influenced further analysis. Average mortality was calculated for each plot for all trees, and for trees at least 10" DBH in excel. Average plot values of NDVI and dNDVI were extracted from imagery in ArcMap 10.1 and explored as potential predictors of both average mortalities in linear regression using JMP Pro 9. Table 4.1 shows the results – in every case, there is a greater correlation between mortality of trees 10" DBH and greater and the given predictor, than between that predictor and overall mortality. The mortality of trees 10" DBH and greater was used for all further analysis.

Table 4.1: Linear fits, overall and 10” DBH mortality

<u>Model</u>	<u>Mortality</u>	<u>R-squared</u>
Quickbird NDVI	Overall	0.169
	10” DBH+	0.373
Quickbird dNDVI	Overall	0.181
	10” DBH+	0.286
NAIP 2010 unshadowed NDVI	Overall	0.441
	10” DBH+	0.480
NAIP 2010 adjusted NDVI	Overall	0.385
	10” DBH+	0.487
NAIP 2012 NDVI	Overall	0.297
	10” DBH+	0.321
Spry 2010 NDVI	Overall	0.360
	10” DBH+	0.385

Plot mortality of trees 10” DBH and greater was coded as a categorical variable to determine the relative effectiveness of using only imagery, using imagery and post-fire LiDAR, and using imagery and pre- and post-fire LiDAR to classify mortality. The categories used and number of plots in each category are shown in table 4.3.

Table 4.2: Plot mortality categories

<u>Mortality of trees 10” DBH and greater (%)</u>	<u>Mortality Class</u>	<u>Number of plots</u>
< 25	Low	20
25-50	Moderate	16
> 50	High	11

These categories were chosen to provide enough information to land managers with as few classes as possible. In areas with less than 25% mortality of trees 10” DBH and greater, salvage harvesting is not likely to be economically viable, and the impact of mortality on the long-term productivity of these areas should be small. In areas with

greater than 50% mortality, harvesting is probably necessary to maintain productivity, and is very likely to be supported from an economic point of view. Areas in between will likely need further assessment based on the age, size, and density of timber, accessibility, and landowner objectives.

The categorical mortality variable was used as the response variable in Classification Analysis and Regression Trees (CART) models in JMP Pro 9. Leave-one-out cross-validation was used. The CART procedure selects variables and values at which to split data in order to maximize homogeneity within the resulting classes. Compared to logistic regression, it is better able to handle non-linearity and multicollinearity, both of which were present in the data. It has the additional benefit that the output is easy to interpret – the decision trees for models are shown in section 4.2.

4.1 Imagery

As stated above, initial, exploratory analysis was done using linear regression. In the case of the Tasseled-Cap-transformed QuickBird, the 'greenness' band has a negative relationship with mortality, while the 'other' band has a positive relationship. In order to capture both effects in a single metric, the difference (greenness-other) was calculated. In addition, to explore whether normalization by brightness would improve any of the relationships, greenness/brightness, other/brightness, and (greenness-other)/brightness were calculated. In the case of the NAIP 2010, where portions of the scene were masked out, as discussed in the methodology section, the relationship between NDVI and mortality was determined to be different for shadowed versus unshadowed pixels, and two strategies were evaluated: using only unshadowed pixels, and using a weighted

average of unshadowed and adjusted shadowed pixels. Figure 4.1 shows the original and adjusted red and infrared bands, and the NDVI as calculated before and after adjustment. Table 4.3 shows the results of all linear regressions against plot percent mortality of trees 10” and greater.

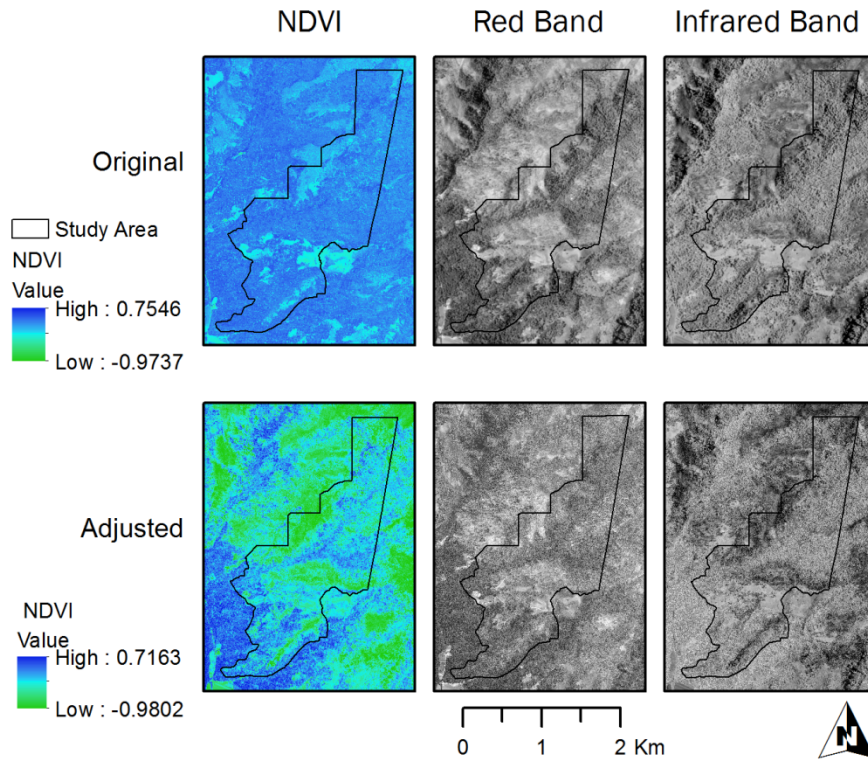


Figure 4.1: 2010 NAIP bands 1 and 4 and NDVI, before and after adjustment

Table 4.3: R^2 and p , linear regression

<u>Model</u>	<u>R^2</u>	<u>p</u>
Quickbird TCT Green/Bright	0.270	0.0002
Quickbird TCT (Green-Other)/Bright	0.264	0.0002
Quickbird TCT Green-Other	0.211	0.0012
Quickbird TCT Green	0.210	0.0012
Quickbird TCT Other/Bright	0.167	0.0044
Quickbird TCT Other	0.144	0.0086
Quickbird NDVI	0.373	<.0001
Quickbird dNDVI	0.286	0.0001
NAIP 2010 NDVI	0.002	0.76
NAIP 2010 unshadowed NDVI	0.480	<.0001
NAIP 2010 adjusted NDVI	0.487	<.0001
NAIP 2010 adjusted NDVI above 1m	0.513	<.0001
NAIP 2010 adjusted NDVI above 2m	0.516	<.0001
NAIP 2010 unshadowed dNDVI	0.314	<.0001
NAIP 2012 NDVI	0.321	<.0001
NAIP 2012 dNDVI	0.233	0.0006
Spry 2010 NDVI	0.385	<.0001

Canopy-height masking (removing pixels which do not represent forest canopy, using masks made from the LiDAR-derived canopy height model) was explored with QuickBird and Spry imagery, but did not improve relationships with mortality. Canopy-height masks at 1-2 m improved the relationships for the 2010 NAIP unshadowed NDVI, but not above 2 m; because the number of pixels retained in the unshadowed NDVI was already low for several plots, the canopy-masked versions, with even fewer pixels contributing, were not used. Relationships for the 2010 NAIP adjusted NDVI *did* continue to improve when masks above 2 m were used, however, again, the number of pixels participating in the average values for some plots became small.

Image metrics with R^2 greater than .25 were used as factors in decision tree classification using leave-one-out cross-validation in JMP Pro 9. The number of trees in each plot was used as the weight. Two models were clearly superior, and, unsurprisingly, they were the models which had the highest R^2 for linear fits: 2010 NAIP unshadowed NDVI, and 2010 NAIP adjusted NDVI above 2 m. Confusion matrices are shown in tables 4.4 and 4.5; both had 74% overall accuracy.

Table 4.4: Confusion matrix, 2010 NAIP unshadowed NDVI

Reference	Classification			Total	Omission error
	< 25%	25-50%	>50%		
< 25%	15	5	0	20	0.25
25-50%	2	13	2	17	0.24
>50%	1	2	7	10	0.30
Total	18	20	9	47	
Commission error	0.17	0.35	0.22		0.26

Table 4.5: Confusion matrix, 2010 NAIP adjusted NDVI above 2m (scheme A)

Reference	Classification			Total	Omission error
	< 25%	25-50%	>50%		
< 25%	19	1	0	20	0.05
25-50%	6	10	1	17	0.41
>50%	0	4	6	10	0.40
Total	25	15	7	47	
Commission error	0.24	0.33	0.14		0.26

Given that the predictive value appears to be roughly the same for the 2010 NAIP NDVI, whether shadowed pixels have their values adjusted or are simply removed, the adjusted version has the advantage that it allows predictions to be made for all pixels. The 2010 NAIP NDVI was chosen for use in fusion with LiDAR data, and for mapping based

on classification (shown in Appendix A) and will be referred to as “scheme A” from here on, for the purposes of comparison.

4.2 LiDAR

Classification was performed in JMP Pro 9 using post-fire LiDAR only, and pre- and post-fire LiDAR (differenced LiDAR), in combination with NAIP 2010 adjusted NDVI above 2m. Using only post-fire LiDAR, the best model (scheme B) used:

- NAIP 2010 adjusted NDVI above 2m (NDVI)
- 50th percentile/mean height of points above 2m (p50/mean)
- 50th percentile/mode height of points above 2m (p50/mode)
- Standard deviation of height of points above 2m (St. Dev.)
- Percent of points in the 16-17m height bin (d17m)

The decision tree for this classification is shown in figure 4.2. Vertical distributions of LiDAR returns for each plot, organized by class according to this classification, can be found in appendix C.

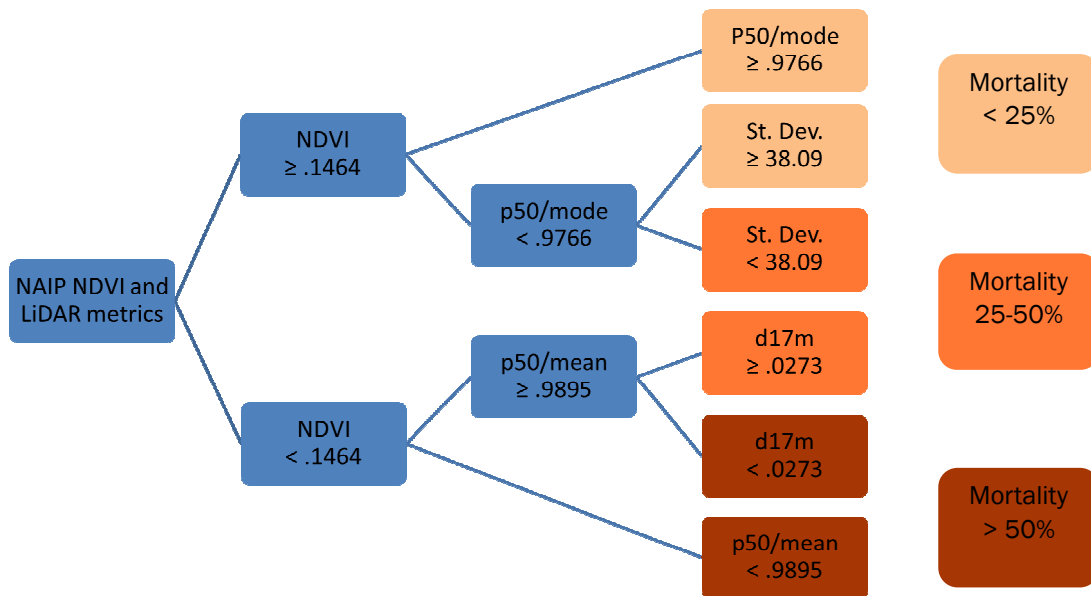


Figure 4.2: Decision tree for Imagery and post-fire LiDAR (scheme B)

The confusion matrix for this model is shown in table 4.6; overall accuracy was 85%.

Table 4.6: Confusion matrix, Imagery and post-fire LiDAR (scheme B)

Reference	Classification			Total	Omission error
	< 25%	25-50%	>50%		
< 25%	17	2	1	20	0.15
25-50%	1	15	1	17	0.12
>50%	0	2	8	10	0.20
Total	18	19	10	47	
Commission error	0.06	0.21	0.20		0.15

Using differenced LiDAR, the best model (scheme C) included:

- NAIP 2010 adjusted NDVI above 2m (NDVI)
- Change in skewness of height of points above 2m (Δskew)
- Change in median of absolute deviations from mode of height of points above 2m ($\Delta\text{MADmode}$)
- Change in percent of points in the 4-5m height bin (Δd5m)
- Change in percent of points in the 6-7m height bin (Δd7m)
- Change in percent of points in the 24-25m height bin (Δd25m)

The decision tree for this classification is shown in figure 4.3.

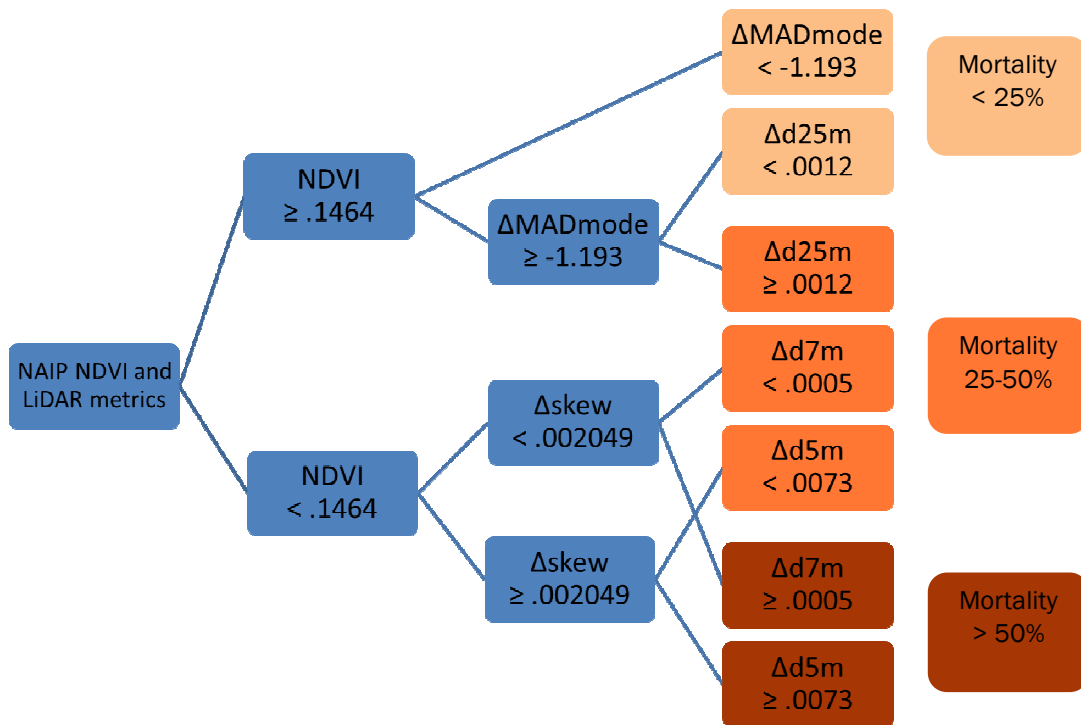


Figure 4.3: Decision tree for Imagery and differenced LiDAR (scheme C)

The confusion matrix for this model is shown in table 4.7; overall accuracy was 83%.

Table 4.7: Confusion matrix, Imagery and differenced LiDAR (scheme C)

Reference	Classification			Total	Omission error
	< 25%	25-50%	>50%		
< 25%	18	2	0	20	0.10
25-50%	1	16	0	17	0.06
>50%	0	5	5	10	0.50
Total	19	23	5	47	
Commission error	0.05	0.30	0.00		0.17

Maps of wall-to-wall estimates of mortality made based on all three schemes can be found in appendix A. For scheme A, the adjusted NAIP 2010 NDVI was used, since the overall accuracy was the same whether shadowed pixels were adjusted or removed, and the adjusted image covers forested area that the clipped image does not. The percent of the fire area by class for each estimate are shown in table 4.8; however, scheme B does not cover the entire fire area due to the extent of the 2008 LiDAR data. For the purpose of making fair comparisons, the other two estimates were clipped to the extent of the 2008 LiDAR data and the percent area recalculated, with the results shown in table 4.9. (The area that is ‘missing’ in the 2008 data is approximately 100 ha, or about 3.5% of the fire area.) Maps showing estimates of mortality by all three schemes for a portion of the study area, including areas which were salvage-harvested, are shown in figure 4.4.

Scheme A had much higher error of omission in the moderate-mortality class than did either of the classifications which used LiDAR data. As shown in tables 4.8 and 4.9, in figure 4.3, and on the maps in appendix A, a greater area is classified as moderate-mortality when LiDAR data are used (much greater in the case of the differenced LiDAR). Scheme C, which had the highest error of omission in the high-mortality class,

has a very small area classified as high-mortality. Generally, the patterns observed on the wall-to-wall predictions mirror what can be seen from the confusion matrices. Although all of the available quantitative data were used in generating these predictions, so that no external validation can be done, we do have some additional qualitative data available, in the form of the salvage harvest area. Salvage harvesting was carried out in areas with a relatively high degree of damage. We would expect to see the shapes of the salvage harvest areas roughly mirrored in the distribution of the higher-mortality classifications. Based on this information, it is apparent that scheme C has missed some areas of high mortality. Between the other two options, results are more mixed: scheme A has much more of the largest salvage-harvest area shown (in the lower half of each frame) classified as high-mortality, however, several smaller areas which were harvested are classified mostly in the low- and moderate-mortality groups, while scheme B has these areas mostly split between the moderate- and high-mortality groups. Moving back to the realm of that which can be measured: aside from having the highest overall accuracy, classification based on post-fire LiDAR has the lowest error of omission in the high mortality class. Given managers' likely preference for errors of commission rather than errors of omission in the highest mortality class, this is probably the best interpretation available based on these data.

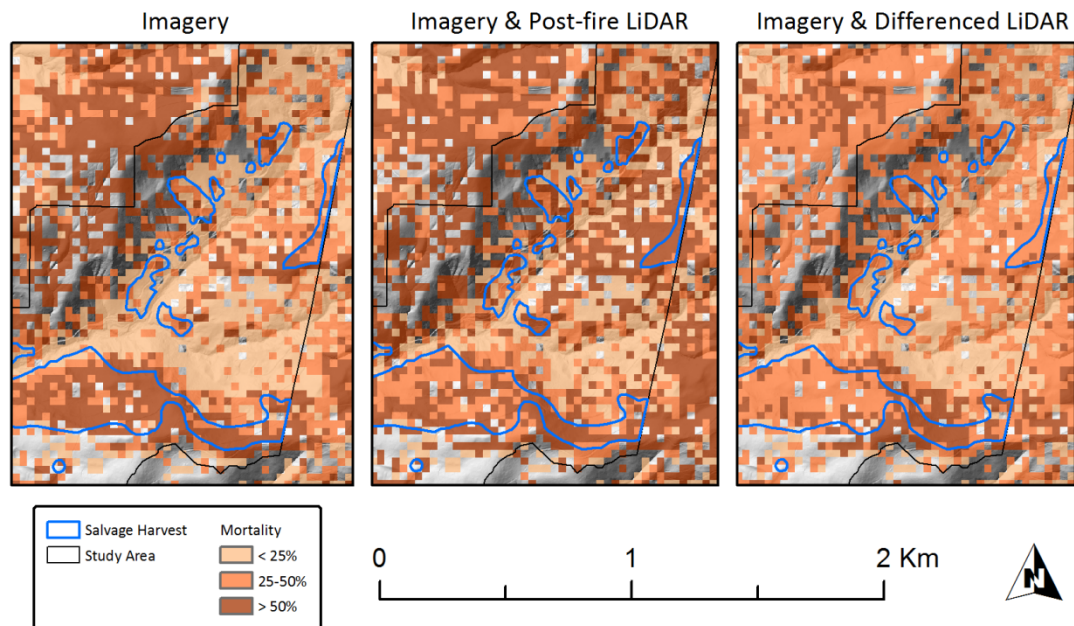


Figure 4.4: Estimated mortality in study area by 3 methods

Table 4.8: Percent area by mortality class, Lockheed Fire

Mortality	Percent of fire area by class		
	Imagery	Imagery + post-fire LiDAR	Imagery + differenced LiDAR
< 25%	42.07	29.02	30.60
25-50%	21.46	25.41	53.22
> 50%	36.47	45.57	16.19

Table 4.9: Percent area by mortality class, clipped to extent of 2008 LiDAR coverage

Mortality	Percent Area		
	Imagery	Imagery + Post-fire LiDAR	Imagery + differenced LiDAR
< 25%	42.26	29.24	30.60
25-50%	20.91	25.29	53.22
> 50%	36.83	45.58	16.19

4.4 Salvage harvesting

One aspect of the data which has not yet been discussed is the potential impact of salvage harvesting on this analysis. Following the fire, salvage harvesting was conducted under an emergency notice before any remote sensing data (except for the QuickBird imagery) were collected. Although limited in scope (10 of the 47 plots used had at least one tree removed; 24 total trees were removed from included plots), this harvesting may have altered the radiometric signature of plots, and almost certainly altered the LiDAR metrics used. In order to assess the likelihood that salvage harvesting affected the results, all metrics chosen by the CART procedure were plotted against mortality of trees 10" DBH and greater, with points coded by salvage harvest status. These plots are shown in figure 4.5. It does not appear that plots which were (or may have been) harvested in the salvage operation have different values for any of the metrics used, or that those values have a different relationship with mortality.

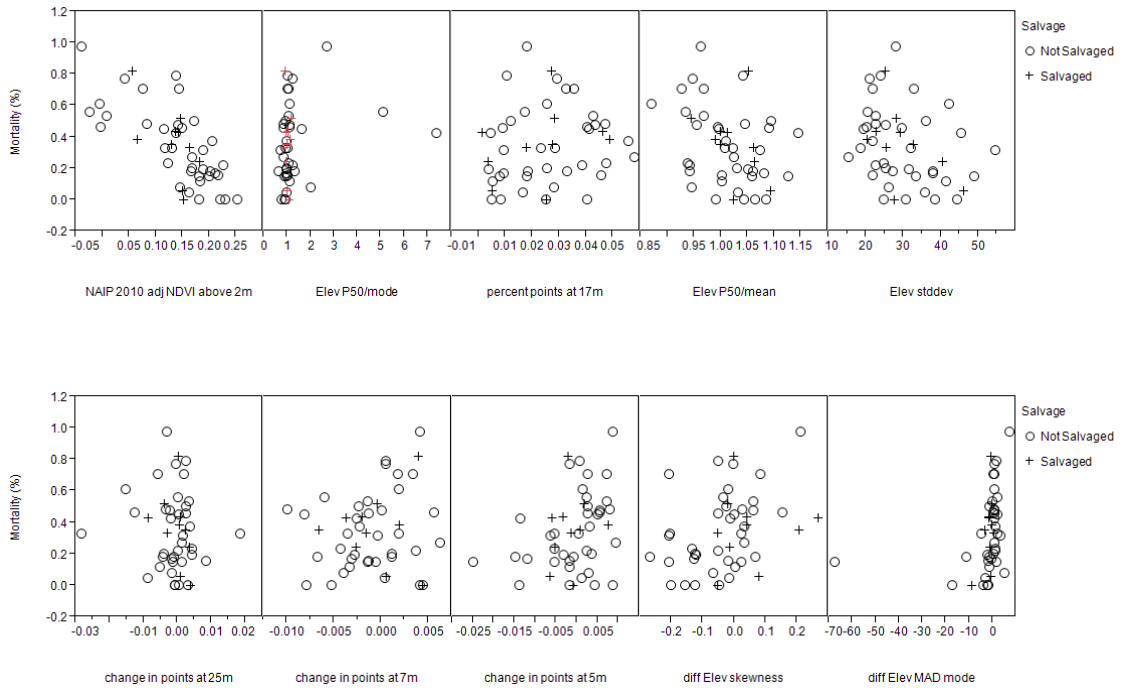


Figure 4.5: Classification metrics vs. mortality by salvage status

As mentioned, QuickBird imagery captured after the fire and before salvage harvesting took place were available. Figure 4.6 shows the NDVI which was used from the NAIP 2010 imagery plotted against the QuickBird NDVI, with plots coded by whether or not they were harvested. A difference due to harvesting would appear as a difference in the relationship between the two NDVIs, which there does appear to be. It is possible, then, that the signal of plots which were harvested is noticeably changed in the NAIP image, however, with only 10 plots, it difficult to be sure of the relationship. Given that the relationship between mortality and NAIP NDVI does not appear to be different, it is reasonable to use the NAIP NDVI instead of the QuickBird.

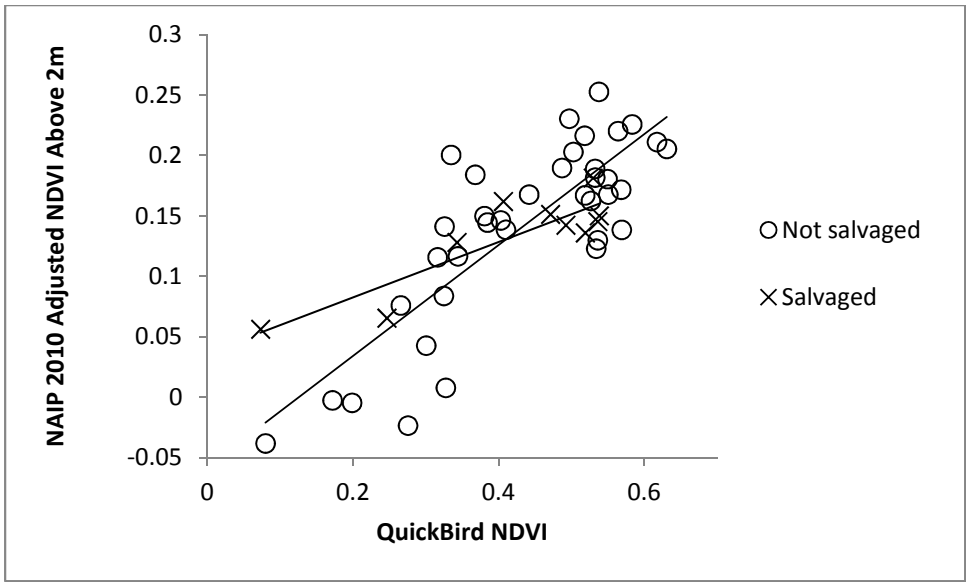


Figure 4.6: NAIP 2010 adj. NDVI above 2 m vs. QuickBird NDVI

Chapter 5

Discussion and Conclusions

This study demonstrates that remote sensing data can be used to estimate plot-level tree mortality resulting from wildfire with a modest degree of accuracy. Using a single, freely available post-fire image, mortality was estimated with 74% accuracy. Although approximately 40% of plots in the higher two mortality classes were misclassified, importantly, no plots with high mortality (> 50%) were classified as low mortality (< 25%), or vice-versa. Examination of the map of this prediction for the entire fire area (Appendix A) suggests that too much area was classified as low-mortality by this method; the confusion matrix suggests that much of this area should have been classified as moderate.

The addition of LiDAR data is associated with significant extra cost unless data gathered for some other purpose happens to be available. At present, the question for anyone considering the use of LiDAR data for predicting mortality or characterizing fire

severity will be whether this extra cost is justified by increased accuracy. As more uses are developed for the data, however, collection becomes more economically feasible. In addition, anecdotally, it appears that the extent of acquisitions is increasing, and the future will likely bring more widely available, higher quality inexpensive or free LiDAR data. In this study, the fusion of imagery with post-fire LiDAR data improved overall accuracy from 74 to 85%. Most of the improvement is in plots which were incorrectly classified as low-mortality and which are in fact moderate-mortality. On the other hand, classification using post-fire LiDAR is less accurate when it comes to low-mortality plots, and classifies one of these plots as high-mortality, which is one of only two plots which were misclassified across two classes – the other being in the unshadowed NDVI classification.

Two of the variables selected in scheme B – p50/mean and p50/mode - describe the skew in the data. The standard deviation is used in combination with p50/mode – where both are low, mortality is higher. Similarly, where the ratio of p50/mean is low, mortality is high, as it is where p50/mean is higher but the percentage of returns from 16-17m is low. To state this another way, for similar values of NDVI, mortality is lower where p50/mean and d17 are high – where there are more returns higher in the canopy, by two different measures.

The fusion of imagery and pre- and post-fire LiDAR in a change-detection approach is not supported by this study. There was a slight decrease in overall accuracy compared to post-fire LiDAR fused with imagery, and this strategy yielded the lowest accuracy in the highest-mortality class of all strategies explored. Half of the plots with mortality greater than 50% were misclassified as moderate-mortality.

Similarly to scheme B, scheme C used variables describing the skew and variation in the data set – in this case, Δskew and $\Delta\text{MADmode}$ – and change in normalized densities in three height bins, from 4-5, 6-7, and 24-25 m. Where $\Delta\text{MADmode}$ was higher (positive or only slightly negative), and Δd_{25m} was positive, mortality was higher, which seems counterintuitive. Where Δd_{7m} and Δd_{5m} were negative, mortality was lower, which seems reasonable if the change was due to more returns higher in the canopy, but this is not certain – it could also be due to a higher proportion of returns below those thresholds.

Unless pre- and post-fire data collections are made with differencing in mind, they will likely differ in density, which affects both DEM generation and canopy metrics in complex ways, interacting with slope and cover. These effects likely confound the relationships between metrics and actual aboveground structure, making relationships with mortality (or other attributes) difficult to detect. In addition, data sets may have been separated into files of manageable sizes using different grids, as was the case in this study. Differences in density and in gridding make calculation of differenced metrics much more complex and time-consuming than metrics from a single dataset. As a result, in most cases, differencing would have to yield a significant improvement in accuracy to justify the additional time and effort.

Outside of statements which have already been made about overall accuracy and accuracy within specific classes, there is no way to evaluate which of the three maps of estimated mortality is the most accurate without collecting additional field data. Between schemes A and B either *appears* plausible, and scheme B is associated with higher overall accuracy. Between schemes B and C, although the overall accuracy of the classifications

is the same, scheme B is likely a better representation. It is difficult to believe that only 16% of the fire area experienced greater than 50% mortality in trees over 10" DBH, and we know from the results that plots with high mortality were misclassified as moderate-mortality. Given the choice between over- and under-estimating mortality, at the same overall accuracy, it is safer to over-estimate. Hypothetically, if salvage harvesting were proposed for all areas with greater than 50% mortality: field verification of the 46% of scheme B classified as high-mortality (1,130 ha) will be quicker than verification of the 16% of scheme B classified as high-mortality (390 ha) *plus* checking the additional 53% (1,280 ha) classified as moderate-mortality, much of which likely experienced mortality over 50% as well.

It is unlikely that the estimates of mortality for the entire fire area based on this study (shown in Appendix A) are the most accurate which could be produced by a similar method. Not only do the 47 plots used represent only 0.12% of the total fire area (0.15% of the area with some canopy above 2m), they are concentrated in a relatively small area of generally similar vegetation. Had the goal of this study been the generation of an accurate estimate of the distribution of mortality across the forested area burned, a larger sample, distributed across space as well as differing forest types, would have been taken. However, using high-quality inventory data which was already available, we have demonstrated the utility of remote sensing data in estimating mortality, and explored the relative value of various methods of interpretation of that data as well as the additive value of LiDAR data.

5.1 Imagery

Imagery alone explained almost half of the variability in mortality that was seen in the field data. Two sets of digital aerial photography and one set of satellite imagery were experimented with in this study. The NAIP photos, which provided the best results (once shadowed pixels were removed or adjusted) have the additional benefit of being the least expensive. The downside to this imagery is that it is collected on a 3-year cycle, so while the timing was good for this study, that will not be the case for the majority of fires. Paying to have an area flown is also an option, as is paying for satellite imagery, both of which were also explored. Collecting aerial photos specifically for use in a project or study has the benefit that the timing of acquisition can be controlled, subject to availability of contractors. While there is a penalty in terms of cost and/or resolution, and likely of accuracy as well (in this study, the satellite images had notably larger errors in the two positions which were checked), satellite imagery has the best temporal resolution, with many satellites covering the entire planet every 14-20 days. This means that, if contractors are not available to fly your project when you want, or if the decision to purchase imagery is made after the optimal window to collect images, satellite imagery may be the best option.

A variety of manipulations of imagery were experimented with as part of this study. Results for NDVI, dNDVI, and tasseled-cap transformations (for QuickBird imagery) can be found in section 4. In general, NDVI was found to be the best predictor of mortality – better than dNDVI, which was somewhat surprising. One likely reason for this is that the before and after images are not phenologically matched as recommended by Key and Benson (2006). Had there been available imagery from the spring of 2009

and 2010, it is possible that dNDVI would have performed better than a simple post-fire NDVI.

The adjustment of shadowed pixel values prior to calculation of NDVI is a novel technique, which was developed on the spot, due to need. A similar technique was used by Sarabandi et. al. (2004), although their method also adjusted for differences in standard deviation. The NDVI was originally developed using Landsat data, which, with a 250 pixel size, does not have the same type of shadows that the data used here, with resolution between 30 cm and 2.4 m, do. Although dividing the difference in bands by the sum is supposed to account for differences in illumination, it would appear that, with much higher resolution data, this is not adequate. The technique used here, or the slightly more involved adjustment used by Sarabandi et. al., may be a necessary step prior to calculation of NDVI from high-resolution imagery with substantial areas of deep shadow.

5.1.1 Spry Imagery

The relatively poor results obtained using the Spry imagery is something of a mystery. The Spry photos were taken at a relatively low elevation, which causes relatively large displacements, but these appear to have been handled well by the orthorectification process. The other result of this process is that the Spry imagery is a mosaic of a greater number of smaller individual scenes. The CFI plots in this study straddle two individual scenes from different flight lines, with slightly different illumination. A sample area from the sidelap of these two scenes was cropped out, and the values of the red and infrared bands examined, as shown in figure 5.1. These pixel values represent the same area, so that any difference is the result of illumination.

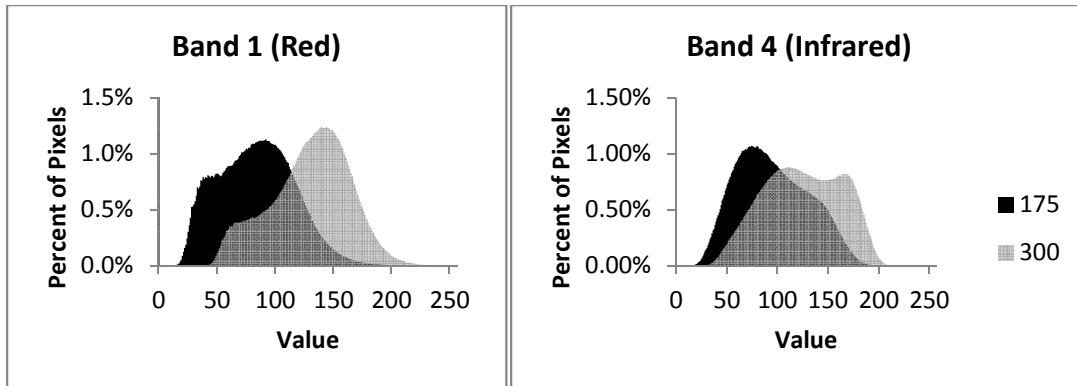


Figure 5.1: Pixel values from sample of Spry images

In theory, calculation of NDVI accounts or controls for differences in illumination. As can be seen in the comparison of NDVI from the same sample area, shown in figure 5.2, there is a difference in values, although it appears smaller in magnitude than that seen in the raw band values. It seems possible that the remaining difference in values, resulting only from differences in illumination, is a factor in the lesser utility of this imagery in explaining variability in mortality.

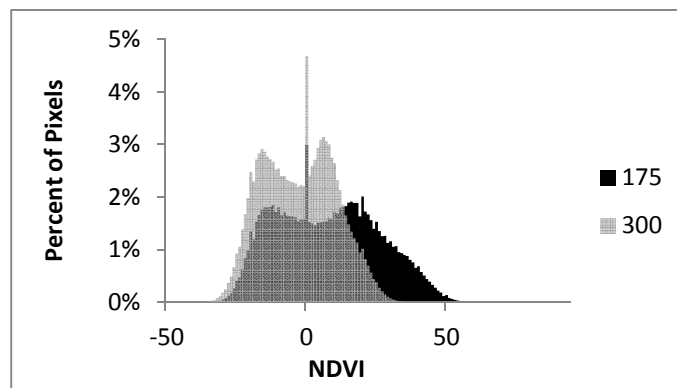


Figure 5.2: NDVI from sample of Spry images

5.1.2 Masking

The simplest fusion of LiDAR data and imagery in this study was the use of

canopy masks generated from LiDAR data to clip imagery to the extent of tree canopies. This technique substantially improved the relationship between NDVI and mortality. While these gains do not, by themselves, justify the collection of LiDAR data, the technique is relatively simple, and, unlike the rest of the analysis, could be done with already existing pre-fire data.

5.2 Limitations and sources of error

5.2.1 Sample size

The primary limitation of this study is the relatively small sample size. The 47 plots used represent only 1.25% of the study area. More importantly, each plot classified represents a change in accuracy slightly over 2%, so that the resolution of the differences in accuracy with different strategies is not particularly fine. Additionally, the minimum number of plots per node, set at 5, was reached in several nodes. A larger sample size would have yielded more resolution and better accuracy in describing the difference in results using different data, as a result of the smaller proportion of the data represented by each plot, as well as greater certainty about the ultimate accuracy of predictions, as a result of a greater number of plots per node.

5.2.3 Spatial accuracy

Plot locations used in this study were measured with a Garmin 60 C Sx, which is a recreational-grade unit. While their ultimate accuracy is lower than that of mapping-grade units, personal experience working in the study area has demonstrated that currently available mapping-grade units will not establish a position in many plot

locations. The accuracy of positions established by recreational-grade units is generally accepted to be less than that of mapping-grade units, but is not the subject of much published literature. However, a similar unit, deployed in forested conditions, had average RMSE of 16.88 m, with the authors calculating 95th percentile RMSE to be 29.22 m (Danskin, Bettinger, Jordan, & Cieszewski, 2009). Using these values, the average plot would have an error representing approximately 64% of the plot area – this is the proportion of the remote sensing data that is outside the field plot. The 95% error stated is nearly equal to the plot diameter – only 3% of the remote sensing data sampled would be from the actual area of the field plot. The consequences of errors in plot locations are probably less than might be suggested by the percentages stated, given that some area immediately outside plots will contain canopies of trees which are in fact located within those plots, while a similar area which is in fact part of the plot will contain canopies of trees which are outside the plot. In addition, fire characteristics and effects cannot be expected to be drastically different over the space of a few meters. Assuming that the first 3 m outside field plots are still a reasonable sample, the average plot's sample has an error of 51% of the sampled area (although a similar percentage of the larger hypothetical field 'plot' is sampled – 35% vs. 36%), while the 95% error of 29.22 m would sample 7% of the 'plot' (9% of the sample data would be within the 'plot'). Figure 5.3 illustrates these example cases.

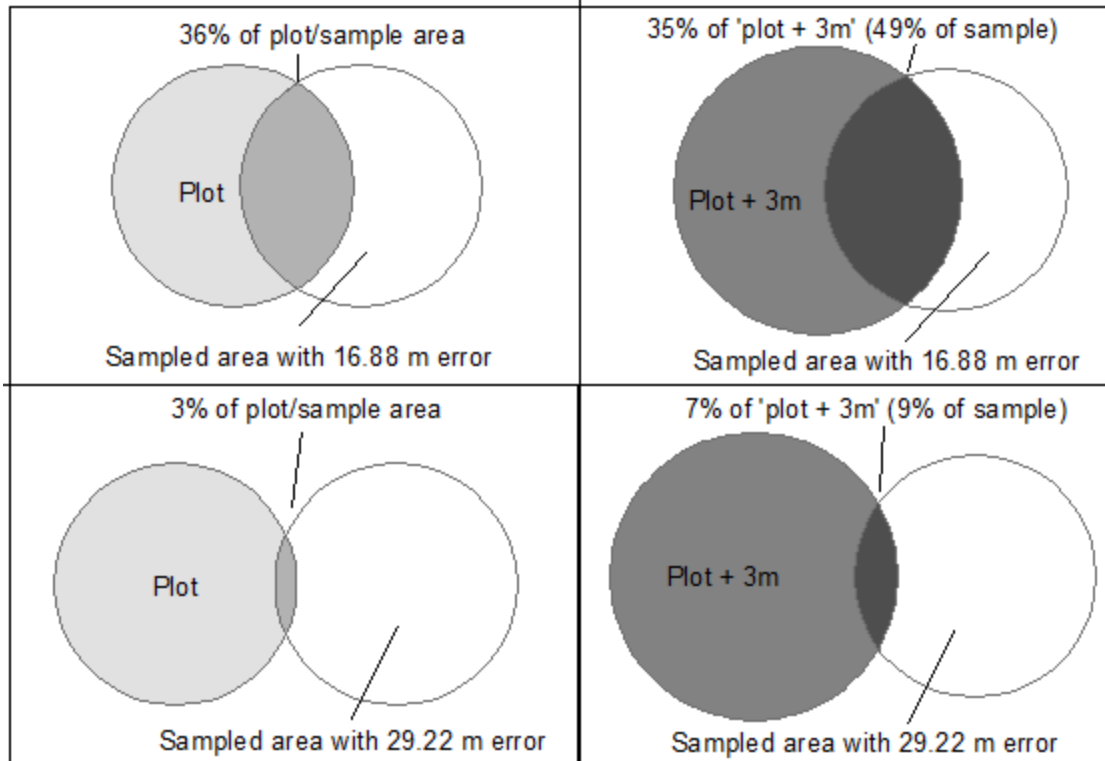


Figure 5.3: Illustration of plot errors and areas

The accuracy of the remote-sensing data used for this study is given in section 3, and is much smaller than the likely errors in plot positions. The two sources of error (error in the data being extracted and error in the locations for which that data was extracted) interact in complex ways in terms of magnitude and direction. Errors may be offsetting or may compound, and a small number of plots could easily have virtually no error, or very large errors. There is no way of saying which plots have more or less, but it seems that, on average, a little more than half of the remote-sensing data used was from areas outside the CFI plots. This almost certainly had a negative effect on the accuracy of predictions. When working with remote sensing data in a forested environment, especially one with rugged topography, it is unrealistic to assume that field and remotely-sensed data can be perfectly matched. Two strategies could have been used to reduce the

amount of error in this study: more exact location of field plots, or larger plots. As mentioned previously, at present, higher-accuracy GPS units are not generally able to establish a position in most of the study area, leaving traditional surveying as the only option to more precisely locate the field plots. After reviewing the condition of the forest after the fire, it was established that this would not be practical, and possibly even unsafe. As for the size of plots, this study used pre-existing plots, so that increasing their size was not possible, however, the use of larger plots is suggested for any future similar studies, to minimize the effects of errors in plot locations and in remote-sensing data.

5.2.4 Salvage harvesting

As discussed in section 4.4, 10 of the 47 plots used in this study were partially harvested prior to collection of remote sensing data. Although it does not appear that harvesting altered the relationship between NDVI and mortality, it is possible that it affected relationships between LiDAR variables and mortality.

5.2.5 Adjustment of NAIP reflectance values

The use of average band values for a sample area to adjust raw values of bands 1 and 4 prior to calculation of NDVI could have introduced some bias into the calculated NDVI values. The facts that plot values were generally similar for clipped vs. adjusted NDVI, and that overall the two performed similarly at predicting mortality, tend to support the notion that adjustment did not negatively influence plot NDVI values.

5.2.6 Errors in mortality data

The mortality data used for this study was collected by student interns and temporary employees at Swanton Pacific Ranch, under the supervision of resource

manager Steve Auten, whose Master's thesis compared the accuracy of initial assessment to that of assessment 3 years following the fire. Overall, initial assessment was 87.9% accurate, including smaller diameter classes which had lower accuracy (Auten, 2012). It can reasonably be assumed that a few trees which were removed during salvage operations may have actually survived the fire, meaning that the percent mortality for a few plots may be slightly inaccurate. In addition, it is possible – although plots were assessed for 3 years and each year's assessments compared to find inconsistencies – that some trees were mistakenly misclassified.

5.3 Recommendations for further study

The relatively small number of plots used in this study precluded the separation of the data into training and validation sets. External validation of the model(s) generated, through the collection of additional mortality data, would provide valuable information about the true accuracy of the models. Data could be gathered from within the study area, or from similar forestland in adjoining watersheds which was subject to the same fire, if adjoining landowners were agreeable, since the data sets used for this study cover the entire burn area (with the exception of the pre-fire LiDAR, which did not prove particularly useful in any case). Alternatively, or in addition, it would be interesting to see if the predictors which were of value in this forest/fire were also the most useful in another fire, in a similar coast redwood forest. There have been several fires in similar forestland in the last ten years. The Martin Fire burned 210 hectares near Bonny Doon, the Summit Fire burned 1,728 hectares near Corralitos, and the Basin Complex Fire burned 659 km² in the Ventana Wilderness of the Los Padres National Forest – all in

2008. Post-fire LiDAR data may be available for at least a portion of some of these areas. It is, of course, possible that another significant forest fire will occur in the next few years in the Santa Cruz mountains. If there were an opportunity to collect LiDAR soon after another fire in the area, it could provide a valuable comparison to this study.

Another approach to estimating mortality would be to model fuels using the combination of imagery and LiDAR data, similar to work by Jakubowski et. al. (2013), and estimate mortality as a result of fire severity by modelling the fire. While this approach is outside the scope of this study, the data are available, and it would be interesting to compare the results of the two approaches.

Works Cited

- Anderson. (n.d.). Continuous Forest Inventory for Swanton's Archibald, Winter, and Western Little Creek Stands. Natural Resources Management Department, California Polytechnic State University San Luis Obispo, CA.
- Auten, S. (2012, December). *Mortality assessment of redwood and mixed conifer forest types in Santa Cruz County following wildfire*. California Polytechnic State University, San Luis Obispo, CA.
- Boer, M. M., Macfarlane, C., Norris, J., Sadler, R. J., Wallace, J., & Grierson, P. F. (2008). Mapping burned areas and burn severity patterns in SW Australian eucalypt forest using remotely-sensed changes in leaf area index. *Remote Sensing of Environment*, 112(12), 4358–4369. doi:10.1016/j.rse.2008.08.005
- Bonner, L. E. (1998). CFI Inventory Report for the Swanton Pacific Ranch. Natural Resources Management Department, California Polytechnic State University San Luis Obispo, CA.

- C. Kenneth Brewer, J. Chris Winne, Roland L. Redmond, David W. Opitz, & Mark V. Mangrich. (2005). Classifying and mapping wildfire severity: a comparison of methods. *Photogrammetric Engineering and Remote Sensing*, 71(11), 1311–1320.
- Carson, W. W. (2004). LiDAR applications in forestry - an overview. *ASPRS Annual Conference Proceedings*.
- Chen, X., Vogelmann, J. E., Rollins, M., Ohlen, D., Key, C. H., Yang, L., ... Shi, H. (2011). Detecting post-fire burn severity and vegetation recovery using multitemporal remote sensing spectral indices and field-collected composite burn index data in a ponderosa pine forest. *International Journal of Remote Sensing*, 32(23), 7905–7927. doi:10.1080/01431161.2010.524678
- Cocke, A. E., Fulé, P. Z., & Crouse, J. E. (2005). Comparison of burn severity assessments using Differenced Normalized Burn Ratio and ground data. *International Journal of Wildland Fire*, 14(2), 189–198.
- Coppin, P., Jonckheere, I., Nackaerts, K., Muys, B., & Lambin, E. (2004). Review Article Digital change detection methods in ecosystem monitoring: a review. *International Journal of Remote Sensing*, 25(9), 1565–1596.
- Danskin, S. D., Bettinger, P., Jordan, T. R., & Cieszewski, C. (2009). A Comparison of GPS Performance in a Southern Hardwood Forest: Exploring Low-Cost Solutions for Forestry Applications. *Southern Journal of Applied Forestry*, 33(1), 9–16.
- Eng, H. (2012). Tree height estimation in Redwood/Douglas-fir stands in Mendocino County (No. Gen. Tech. Rep. PSW-GTR-238) (pp. 649–654). Albany, CA.

- Epting, J., Verbyla, D., & Sorbel, B. (2005). Evaluation of remotely sensed indices for assessing burn severity in interior Alaska using Landsat TM and ETM+. *Remote Sensing of Environment*, 96(3–4), 328–339. doi:10.1016/j.rse.2005.03.002
- Escuin, S., Navarro, R., & Fernández, P. (2008). Fire severity assessment by using NBR (Normalized Burn Ratio) and NDVI (Normalized Difference Vegetation Index) derived from LANDSAT TM/ETM images. *International Journal of Remote Sensing*, 29(4), 1053–1073. doi:10.1080/01431160701281072
- Falkowski, M. J., Evans, J. S., Martinuzzi, S., Gessler, P. E., & Hudak, A. T. (2009). Characterizing forest succession with lidar data: An evaluation for the Inland Northwest, USA. *Remote Sensing of Environment*, 113. doi:10.1016/j.rse.2009.01.003
- Fox, D. M., Maselli, F., & Carrega, P. (2008). Using SPOT images and field sampling to map burn severity and vegetation factors affecting post forest fire erosion risk. *CATENA*, 75(3), 326–335. doi:10.1016/j.catena.2008.08.001
- Goerndt, M. E., Monleon, V. J., & Temesgen, H. (2010). Relating Forest Attributes with Area- and Tree-Based Light Detection and Ranging Metrics for Western Oregon. *Western Journal of Applied Forestry*, 25, 105–111.
- Golinkoff, J., Hanus, M., & Carah, J. (2011). The use of LiDAR and high-resolution imagery to estimate carbon stocks for a verified forest carbon offset project. *Carbon Balance and Management*, 6, 37. doi:10.1186/1750-0680-6-9
- Hill, R. A., & Broughton, R. K. (2009). Mapping the understorey of deciduous woodland from leaf-on and leaf-off airborne LiDAR data: A case study in lowland Britain. *Isprs Journal of Photogrammetry and Remote Sensing*, 64, 223–233.

- Jakubowski, M. K., Guo, Q. H., Collins, B., Stephens, S., & Kelly, M. (2013). Predicting Surface Fuel Models and Fuel Metrics Using Lidar and CIR Imagery in a Dense, Mountainous Forest. *Photogrammetric Engineering and Remote Sensing*, 79, 37–49.
- Kaufmann, M. R., Stoker, J. M., & Greenlee, S. K. (n.d.). Using Lidar to identify sediment and forest structure change in the Hayman burn, Colorado. Final Report, Joint Fire Sciences Program Project No. 03-2-3-18.
- Kauth, R. J., & Thomas, G. S. (1976). The tasseled cap -- a graphic description of the spectral-temporal development of agricultural crops as seen by landsat.
- Kelly, M., Shaari, D., Guo, Q. H., & Liu, D. S. (2004). A comparison of standard and hybrid classifier methods for mapping hardwood mortality in areas affected by “sudden oak death.” *Photogrammetric Engineering and Remote Sensing*, 70. Retrieved from ://WOS:000224887600006
- Key, C. H., & Benson, N. C. (2006). *Landscape Assessment* (p. 51). US Forest Service.
- Kim, Y., Yang, Z. Q., Cohen, W. B., Pflugmacher, D., Lauer, C. L., & Vankat, J. L. (2009). Distinguishing between live and dead standing tree biomass on the North Rim of Grand Canyon National Park, USA using small-footprint lidar data. *Remote Sensing of Environment*, 113, 2499–2510. doi:10.1016/j.rse.2009.07.010
- Kobziar, L., Moghaddas, J., & Stephens, S. L. (2006). Tree mortality patterns following prescribed fires in a mixed conifer forest. *Canadian Journal of Forest Research- Revue Canadienne De Recherche Forestiere*, 36, 3222–3238. doi:10.1139/x06-183

- Leckie, D. G., Cloney, E., & Joyce, S. P. (2005). Automated detection and mapping of crown discolouration caused by jack pine budworm with 2.5 m resolution multispectral imagery. *International Journal of Applied Earth Observation and Geoinformation*, 7. doi:10.1016/j.jag.2004.12.002
- Lee, B., Kim, S. Y., Chung, J., & Park, P. S. (2008). Estimation of fire severity by use of Landsat TM images and its relevance to vegetation and topography in the 2000 Samcheok forest fire. *Journal of Forest Research*, 13(4), 197–204.
doi:http://dx.doi.org.ezproxy.lib.calpoly.edu/10.1007/s10310-008-0072-x
- Lefsky, M. A., Cohen, W. B., Parker, G. G., & Harding, D. J. (2002). Lidar Remote Sensing for Ecosystem Studies. *BioScience*, 52(1), 19.
- Lim, K., Treitz, P., Wulder, M., St-Onge, B., & Flood, M. (2003). LiDAR remote sensing of forest structure. *Progress in Physical Geography*, 27(1), 88–106.
- Lu, D., Mausel, P., Brondízio, E., & Moran, E. (2004). Change detection techniques. *International Journal of Remote Sensing*, 25(12), 2365–2401.
- Maltamo, M., Packalen, P., Yu, X., Eerikainen, K., Hyypä, J., & Pitkanen, J. (2005). Identifying and quantifying structural characteristics of heterogeneous boreal forests using laser scanner data. *Forest Ecology and Management*, 216, 41–50.
doi:10.1016/j.foreco.2005.05.034
- Martinuzzi, S., Vierling, L. A., Gould, W. A., Falkowski, M. J., Evans, J. S., Hudak, A. T., & Vierling, K. T. (2009). Mapping snags and understory shrubs for a LiDAR-based assessment of wildlife habitat suitability. *Remote Sensing of Environment*, 113(12), 2533–2546. doi:10.1016/j.rse.2009.07.002



- Maskrey, & Reimer. (1993). Implementation of Single Coordinate System for Swanton Pacific Ranch. Natural Resources Management Department, California Polytechnic State University San Luis Obispo, CA.
- Meng, Q. M., & Meentemeyer, R. K. (2011). Modeling of multi-strata forest fire severity using Landsat TM Data. *International Journal of Applied Earth Observation and Geoinformation*, 13, 120–126. doi:10.1016/j.jag.2010.08.002
- Muss, J. D., Mladenoff, D. J., & Townsend, P. A. (2011). A pseudo-waveform technique to assess forest structure using discrete lidar data. *Remote Sensing of Environment*, 115, 824–835. doi:10.1016/j.rse.2010.11.008
- Mutlu, M., Popescu, S. C., Stripling, C., & Spencer, T. (2008). Mapping surface fuel models using lidar and multispectral data fusion for fire behavior. *Remote Sensing of Environment*, 112, 274–285. doi:10.1016/j.rse.2007.05.005
- Pasher, J., & King, D. J. (2009). Mapping dead wood distribution in a temperate hardwood forest using high resolution airborne imagery. *Forest Ecology and Management*, 258. doi:10.1016/j.foreco.2009.07.009
- Patterson, M. W., & Yool, S. R. (1998). Mapping fire-induced vegetation mortality using landsat thematic mapper data: A comparison of linear transformation techniques. *Remote Sensing of Environment*, 65. doi:10.1016/s0034-4257(98)00018-2
- Renslow, M. (2000). Evaluation of multi-return LiDAR for forestry applications (No. RSAC-2060/4810-LSP-0001-RPT1) (p. 17). Salt Lake City, UT: Remote Sensing Applications Center, United States Forest Service.

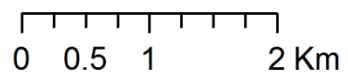
- Rogan, J., & Yool, S. R. (2001). Mapping fire-induced vegetation depletion in the Peloncillo Mountains, Arizona and New Mexico. *International Journal of Remote Sensing*, 22(16), 3101–3121.
- Sarabandi, P., Yamazaki, F., Matsuoka, M., & Kiremidjian, A. (2004). Shadow Detection and Radiometric Restoration in Satellite High Resolution Images. *Geoscience and Remote Sensing Symposium, IGARSS '04 Proceedings, vol. 6*, 3744-3747.
doi:10.1109/IGARSS.2004.1369936
- Wang, C., & Glenn, N. F. (2009). Estimation of fire severity using pre- and post-fire LiDAR data in sagebrush steppe rangelands. *International Journal of Wildland Fire*, 18(7), 848–856.
- White, J.C., Wulder, M. A., Varhola, A., Vastaranta, M., Coops, N. C., Cook, B. D., Pitt, D., & Woods, M. (2013). A best practices guide for generating forest inventory attributes from airborne laser scanning data using an area-based approach.
Retrieved from <http://cfs.nrcan.gc.ca/publications?id=34887>
- Yarbrough, L. D., Easson, G., & Kuzmaul, J. S. (2005). QuickBird 2 tasseled cap transform coefficients: a comparison of derivation methods (Vol. 16, pp. 23–27). Presented at the Pecora.

Appendix A

False-color Infrared Area Map



-  Swanton Pacific Ranch
-  Lockheed Fire perimeter

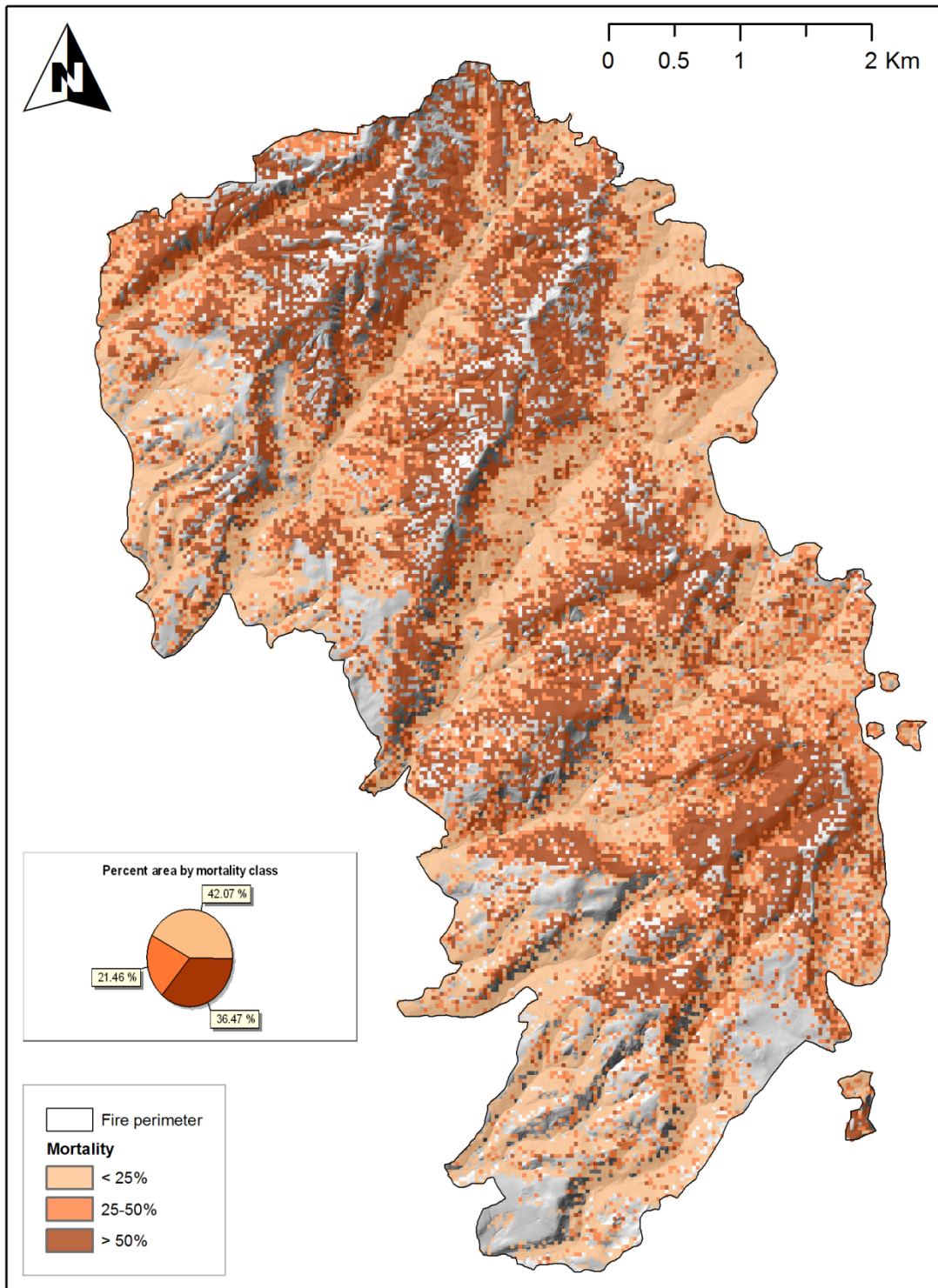


False-color infrared QuickBird imagery collected 9/15/2009

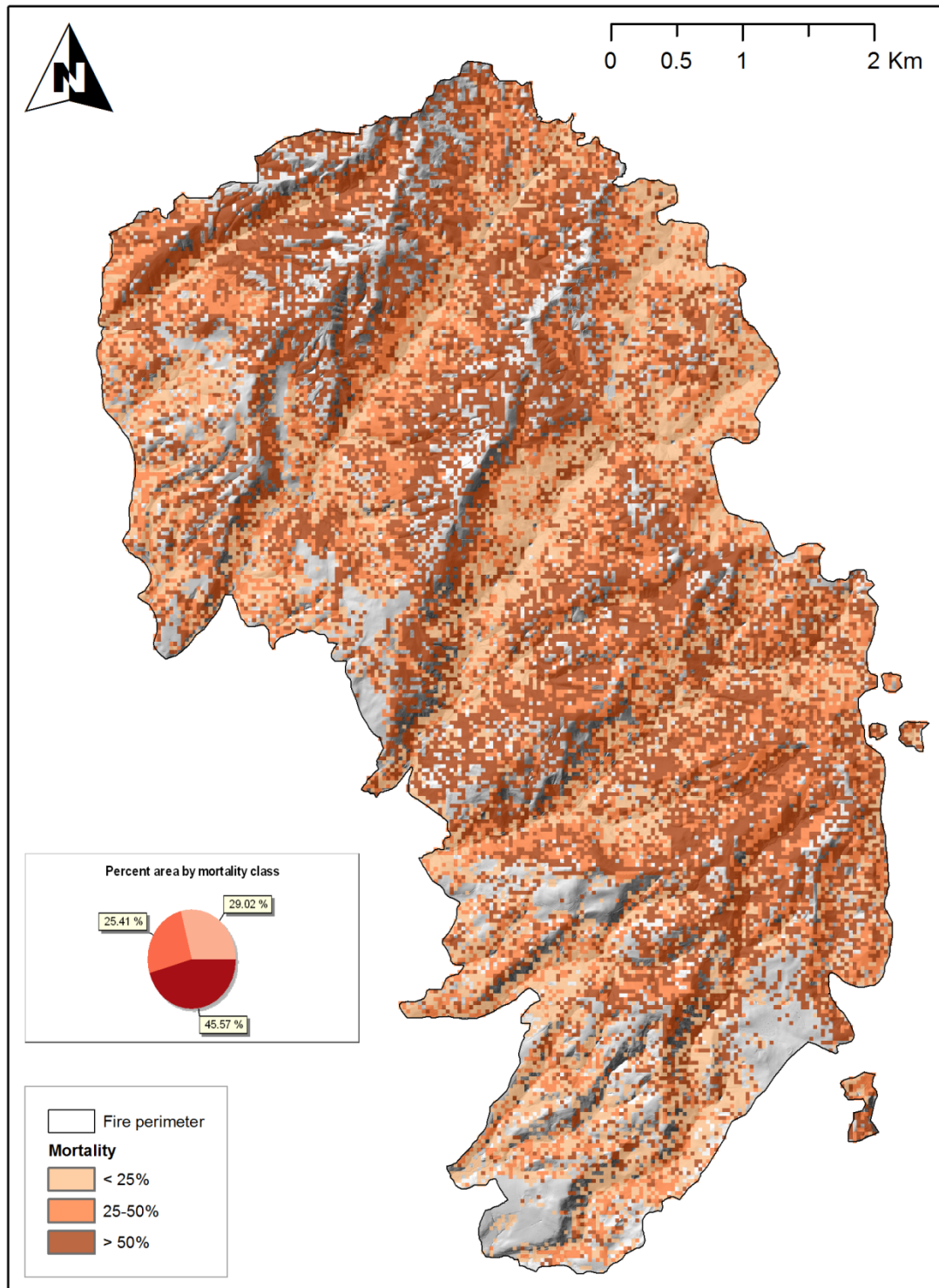
Appendix B

Maps of Estimated Mortality

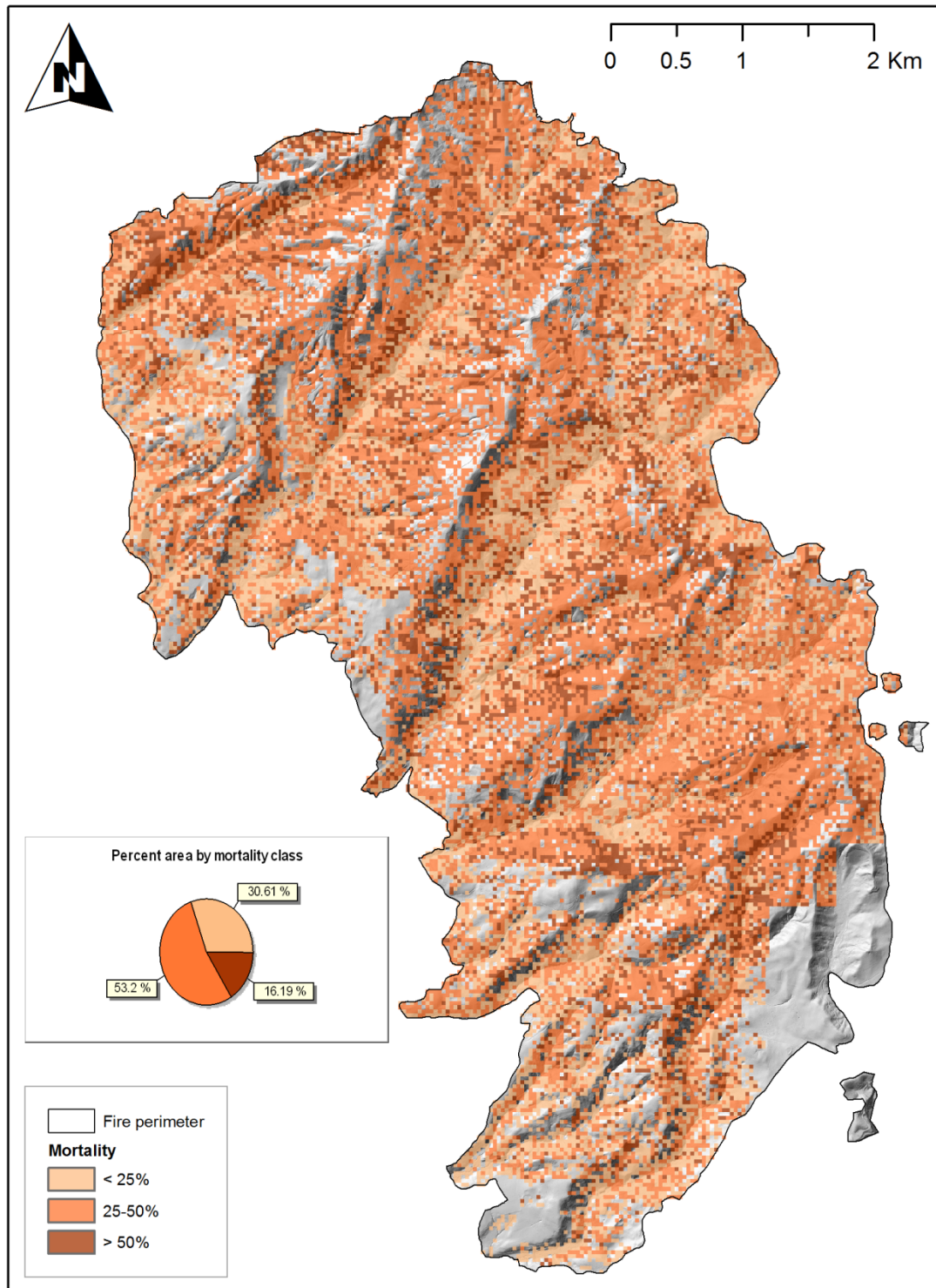
**Percent mortality of trees 10" DBH and greater
from NAIP 2010 Imagery
Lockheed Fire, Santa Cruz County, CA**



Percent mortality of trees 10" DBH and greater from NAIP 2010 Imagery and post-fire LiDAR Lockheed Fire, Santa Cruz County, CA



**Percent mortality of trees 10" DBH and greater
from NAIP 2010 Imagery and pre- and post-fire LiDAR
Lockheed Fire, Santa Cruz County, CA**



Appendix C

Imagery Georeferencing Accuracy Data

Coordinate values are in State Plane Coordinate System, CA zone III:

<u>Image</u>	<u>Northing (ft)</u>	Staub House		<u>Diff</u>	<u>Error (ft)</u>
		<u>Diff</u>	<u>Easting (ft)</u>		
NAIP 2009	1,850,807.99	(0.81)	6,060,396.39	(0.82)	1.16
NAIP 2010	1,850,804.17	3.01	6,060,388.75	6.82	7.45
NAIP 2012	1,850,806.61	0.57	6,060,384.93	10.64	10.65
QuickBird 2008	1,850,789.59	17.59	6,060,421.73	(26.17)	31.53
QuickBird 2009	1,850,814.94	(7.76)	6,060,359.23	36.33	37.15
Spry 2010	1,850,810.08	(2.90)	6,060,395.35	0.22	2.91
		<u>Surveyed values</u>			
	1,850,807.18		6,060,395.56		

Red House

<u>Image</u>	<u>Northing (ft)</u>	<u>Diff</u>	<u>Easting (ft)</u>	<u>Diff</u>	<u>Error (ft)</u>
NAIP 2009	1,850,132.37	(3.26)	6,057,786.93	4.26	5.37
NAIP 2010	1,850,125.01	4.10	6,057,782.96	8.23	9.19
NAIP 2012	1,850,133.21	(4.10)	6,057,786.65	4.54	6.11
QuickBird 2008	1,850,136.24	(7.13)	6,057,760.67	30.52	31.34
QuickBird 2009	1,850,190.40	(61.29)	6,057,641.57	149.62	161.69
Spry 2010	1,850,130.92	(1.81)	6,057,786.85	4.34	4.71

Surveyed values

1,850,129.11 6,057,791.19

Appendix D

LiDAR Height Distributions, scheme B

